Interface between End-Functionalized PEO Oligomers and a Silica Nanoparticle Studied by Molecular Dynamics Simulations

Delphine Barbier,† David Brown, Anne-Cécile Grillet, and Sylvie Neyertz*

Laboratoire Matériaux Organiques à Propriétés Spécifiques (LMOPS), UMR 5041 CNRS-Université de Savoie, Bât IUT, Campus Scientifique, 73376 Le Bourget-du-Lac, France

Received December 19, 2003; Revised Manuscript Received March 31, 2004

ABSTRACT: Fully atomistic molecular dynamics (MD) simulations have been carried out on a series of bulk melt pure PEO oligomers and PEO oligomer−silica systems, which differed by their macromolecular end groups. A realistic hybrid model of a silica nanoparticle combining an ionic core as well as the fine-tuning of the surface thickness and number of OH groups per unit surface area was used. The PEO oligomers were decorrelated in all systems under study in order to prevent any artifacts related to the preparation procedure. Significant changes were found to occur in the immediate vicinity of the interface with flattened PEO backbones arranged in densily packed shells and stabilized by the added PEO−silica interactions. Their conformations were also more coiled in order to better adapt to the surface structure. While methyl end groups did not show special characteristics other than their steric effect, hydroxyl end groups had a much higher affinity for the surface and tended to position themselves perpendicular to the surface, thus forming dynamic hydrogen-bonding complexes between the hydroxyl oxygens and the silanol hydrogens. The range of influence of the nanoparticle was evident for structural properties only up to two or three molecular layers, 10−15 Å, but was approximately twice that for dynamical ones.

1. Introduction

Polymers such as poly(ethylene oxide) (PEO) can be used as dispersants for silica particles.[1,2] Adsorption is thought to occur through hydrogen bonding between the free silanol groups on the silica surface and the ether oxygens of the PEO molecules.[3−5] Although bridging flocculation can happen when high molecular weight PEO is used,[5−8] smaller polymer molecules will saturate the silica surfaces and stabilize the systems.[9,10] This prevents agglomeration and leads to a good dispersion of the silica particles, a property that has numerous applications in material, pharmaceutical and biological fields.[11] Some examples are the water-based latex formulations, where PEO can adsorb both on the silica and on the latex in order to control the colloidal stability of the dispersions and the behavior during the film-processing steps.[12,13]

Many parameters such as polymer chain lengths and molecular weights, particles sizes and distributions, ionic strength and pH of the medium, surface chemistry, etc. are known to influence the adsorption of PEO on the silica surface.[2,10,11,14−21] Another key feature is the importance of chain end groups for chains of the same molecular weight. In a microcalorimetric study, two PEO oligomers of average molecular weight 400 which only differed by their end groups (one being dihydroxylated and the other one dimethylated), were found to exhibit different adsorption isotherms.[14] Competitive adsorption of fluorescein-dianion-terminated PEO (F-PEO) and the corresponding native PEO showed that the latter was favored because of electrostatic repulsions between F-PEO and the silica surface.[22] Alkane-end-capped-PEO adsorption resulted in a tightly adsorbed underlayer related to the backbone ether groups−silanol hydrogen bonds and in a loosely bound outer layer due to the hydrophobic interactions between the chain ends.[23]

Many adsorption results have been linked to conformational changes of the macromolecules close to the silica surface. Brewster angle reflectivity measurements of the adsorbed PEO layer density suggest that the chains will lie flat on the surface at low coverages while the conformations will exhibit more loops and tails at higher coverages.[24] Likewise, dynamic light scattering data,[12] electron spin resonance spectra of spin-labeled PEO,[25] and fluorescence spectroscopy of pyrene-labeled PEO[26] show that the macromolecules tend to extend away from the silica surface into solutions in the form of loops and tails. The effect of terminal groups was also noted in that respect by the two-plateau adsorption isotherms for hydroxyl-terminated low-molecular weight PEO, where it was assumed that hydroxyl end groups would allow the PEO molecules to partially stand up with respect to the silica surface at maximum adsorptions, thereby allowing for the adsorption of more PEO.[14,19,20,27] More recently, sum frequency generation (SFG) vibrational spectroscopy revealed that liquid PEO oligomers exhibit very different conformations depending on the nature of the interfaces.[28] Since these authors could only detect weak SFG signals using methyl-terminated PEO with fused silica, they concluded that the hydrophilic silica and the hydrophobic segments of PEO induce either the macromolecules to have a random structure or the CH_2 and CH_3 groups to lie down at the interface.[28] The potentially different conformations of the polymer on the surface have been suggested as being significant factors for the viscosity of the colloidal suspensions[27] and the increase in elasticity of PEO−silica nanocomposites during thermal annealing.[29]

The aim of the present work is to use molecular simulations methods as a complement to experiments in order to investigate at the atomistic level the char-

* To whom correspondence should be addressed. E-mail: Sylvie.Neyertz@univ-savoie.fr.

† Present address: Lab. de Rhéologie des Matières Plastiques, Faculté des Sciences et Techniques, 23 rue du Dr Paul Michelon, 42023 St-Etienne Cedex 2, France.

10.1021/ma0359537 CCC: $27.50
Published on Web 05/19/2004

acteristics of interfaces between silica and end-functionalized PEO oligomers. Molecular dynamics (MD) simulations[30] integrate Newton's equations of motion for all the atoms in a system and can thus provide direct structural and dynamical information. However, a prerequisite of any realistic MD simulation is a good model, and very complex preparation procedures and interaction potentials will be needed to properly represent such interfaces. It is also worth noting that full-potential MD simulations are usually restricted to one or relatively few nanoparticles in a polymer matrix because of periodic boundary conditions and the need for expensive computer resources. As such, much faster Monte Carlo (MC) simulations[31] are a very useful tool to describe many particles in these systems.

Several approaches to model solid nanoparticles embedded in a polymer matrix have been recently reported. Most of them use particles of different geometric forms and without atomistic details (please note that we restrict ourselves here largely to fairly spherical fillers and do not consider particular cases such as, for example, nanotubes[32]). Lattice Monte Carlo simulations have been used to study phase diagrams of simple cubic particles−diblock copolymers mixtures as a function of particle size and concentration,[33] as well as the behavior of a cubic and a spherical nanoparticle in ordered structures of diblock copolymers.[34] Vacatello has carried out extensive MC calculations of dense polymer melts containing solid spherical nanoparticles in continuous space.[35−40] In his work, the size of the filler particles is comparable to that of the polymer chains, and the conformational distributions of the latter are similar to those of real polymethylene melts.[35] Polymer units in contact with particles are found to form densely packed and ordered shells with specific conformations and overall reduced mobility.[35] Each particle is in contact with many different polymer chains, and each chain can visit the interface shell of several filler particles. Indeed, chains can be considered as sequences of interface, bridge and loop segments, whose relative proportions depend on the volume fraction and size of the filler[36] and which can approximately be predicted[40] (except in the case of large particles and small filling densities[39]). However the chain characteristic ratio is only slightly reduced with respect to the unfilled polymer.[37] Other off-lattice MC investigations with hard sphere nanoparticles include the investigation of the conformation of the complex formed between a positively charged filler and a polyampholyte chain.[41] Molecular dynamics simulations of polymer−filler systems tend to confirm the results obtained by Monte Carlo calculations. The work of Starr et al.[42−44] is based on an icosahedral particle designed to capture the general features of traditional filler particles such as carbon black and surrounded by polymer chains of 20 monomers interacting via a Lennard-Jones (LJ) potential. The macromolecules in the neighborhood of the particle adopt a more elongated and flattened structure than in the melt.[42,43] The chain dynamics and glass transition temperature are also strongly influenced by the nanoparticle. Indeed, both can be modified by controlling the surface interactions and the filler volume fraction.[43] Smith et al.[45] have simulated a roughly spherical nanoparticle in a matrix of 10−20 bead-necklace polymer chains to address more specifically the viscoelastic properties of such systems. In their work, the dynamic shear modulus and the viscosity are found to be strongly affected by nanoparticle volume fractions, specific nanoparticle−polymer interfacial areas and the nature of polymer-nanoparticle interactions.[45] A new development is to use these fairly coarse-grained models to investigate particle−particle interactions and dispersion in nanocomposites using MD simulations. Starr et al. have also now addressed the possible mechanisms of particle clustering by combining up to 125 smaller and simpler icosahedral particles with shorter polymer chains.[44] Similar simulations with several spherical particles in polymers have been conducted by Smith et al. in order to investigate the influence of polymer molecular weights and polymer-particle interaction strengths on aggregation or dispersion of the fillers.[46]

Such multiparticle work with particles of atomistic detail is presently out of reach, mostly because of the enormous CPU times needed when more complicated interactions are taken in account. A PEO chain of a few hundred monomers has been reported to coordinate a small Al_2O_3 particle of diameter ∼2 nm derived from corundum and thus to promote lithium mobility in other regions.[47,48] Brown et al. have carried out much larger MD simulations of a silica nanoparticle of diameter ∼4.4 nm embedded in a 30000-sites united-atom CH_2 matrix.[49] In that work, the silica nanoparticle is modeled as explicit O and Si atoms interacting with each other or with the polymer CH_2 groups through excluded-volume and electrostatic interactions. As seen with simpler particles, the CH_2 segments have a strong tendency to align parallel to the interface and form several structured layers with a distinct gradient and with slightly limited mobility.[49] A more realistic model of the silica particle, consisting of an amorphous core linked to a surface coating, was then designed by Brown et al. and inserted into a ∼26400-atom model of PBMA in order to compare MD simulations to real PBMA−silica composites.[50,51] Although some structuring of PBMA at the vicinity of the particle is visible, the long and relatively stiff polymer chain was found to adapt badly to the inclusion on the MD time scale and remained highly correlated to its starting structure.[50,51]

In this paper, we build on that experience by using a similar realistic model of the silica nanoparticle to that of Brown et al.[50,51] (see later for details), but by considering much shorter and flexible PEO chains so that complete decorrelation can occur on the nanosecond time scale available to standard MD simulations. Two types of end groups will be considered, i.e. $-CH_3$ and $-OH$, and the behavior of these different PEO chains will be compared with the experimental evidence cited above.[14,19,20,27,28] Indeed, limited molecular weight is known to promote denser adsorbed layers[11,52] and the influence of the end groups will certainly be less negligible than for higher molecular weights.[14] Another point is that, although solvents such as water are known to compete with PEO for the silanols surface,[4] the PEO/silica interfaces will here be characterized on their own. We intend to add water to the models at a later stage. We also note that very short 20 ps MD simulations of PEO−silica have earlier been carried out in vacuo to complement small-angle neutron scattering results.[10] In a first simulation, one 40-monomer PEO chain was found to wrap itself tightly around a smaller silica particle created by folding circular chains of Si−O−Si atoms, thus leading to an unsaturated surface consistent with particle bridging. In a second simulation, three 25-monomer PEO chains adopted more extended con-

formations and a greater thickness around a particle of similar size, i.e., closer to a more saturated surface.[10] In our models, complete intermolecular interactions as well as a specific procedure for the preparation of the silica nanoparticle and the relaxation of initial PEO conformations will be included. Finally, we point out the recent work of Borodin et al.,[53] which was carried out on a model of PEO close to a planar crystalline TiO_2 surface. Although the geometry is different, this study is evidently of particular interest since it applies to the same polymer matrix. Comparisons with the work of Borodin et al.[53] will thus be made at the relevant points in the text.

The details of the simulations are given in section 2, while the results are analyzed and discussed in section 3.

2. Computational Details

All simulations were performed using the *gmq* suite of programs[54] on the SGi ORIGIN 3800 and the IBM SP of the CINES (Montpellier, France), the IBM Regatta of the IDRIS (Orsay, France) supercomputing centers as well as on local SGi machines and a COMPAQ DS20E at the University of Savoie (Le Bourget-du-Lac, France). When running on parallel machines, eight processors were used.

2.1. PEO Melts. As explained above, PEO oligomers with two different end groups were considered. The basic chemical structures consisted of nine ($-CH_2-CH_2-O$) monomers, following preliminary results that showed that these chain lengths could be totally decorrelated on a time scale of ∼1−2 ns in the pure bulk melt at 400 K. The respective end groups were either CH_3-CH_2- or $OH-CH_2-CH_2-$, and an oxygen was added so that both ends for a given chain were identical.

The following names will be used throughout the paper to distinguish both types of PEO:

(a) "dimethyl PEO", $H-CH_2-CH_2-O-(CH_2-CH_2-O)_9-CH_2-CH_2-H$

(b) "dihydroxyl PEO", $HO-CH_2-CH_2-O-(CH_2-CH_2-O)_9-CH_2-CH_2-OH$

We have previously developed a fully atomistic model for PEO by accurately reproducing its experimental crystalline structure.[55] This model, extended to dimethyl PEO, gives amorphous densities and diffusion coefficients in reasonable agreement to experiment.[56,57] The potential has also been shown[56] to give characteristic ratios in the melt in agreement with SANS experiments and a different model of PEO.[58]

The potential energy of the chain is described in terms of angle-bending deformations, torsional motions around the backbone dihedral angles, van der Waals and electrostatic interactions. The last two terms represent the so-called "nonbonded" potentials and are taken into account for all intramolecular atom pairs separated by more than three bonds, as well as for atoms belonging to different molecules. High-frequency bond stretching modes are removed by rigidly constraining all bond lengths, and other degrees of freedom involving H atoms are frozen out according to the SHAKE routine[59,60] with a relative tolerance of 10^{-6}. This consists of holding the planes of the rigid $C_\alpha H_2$ groups perpendicular to the planes of the backbone $C-C_\alpha-O$ groups, while fixing CH_3 groups in a rigid tetrahedral geometry. The use of these rigid constraints can be justified by the IR and Raman spectra of PEO, which show that backbone bending and torsions are sufficiently decoupled from the higher frequency modes.[61]

The parameters for dimethyl PEO were identical to those reported before,[55,56] except for the van der Waals interactions which were initially described by the Buckingham form of the excluded-volume potential. As it is eventually intended to add water molecules in such models, the Lennard-Jones form of the excluded-volume potential, $U_{LJ}(r)$, was used instead:

$$U_{LJ}(r) = 4\epsilon((\sigma/r)^{12} - (\sigma/r)^6) \quad (1)$$

Table 1. Composition and Acronyms of the Six Systems under Study[a]

acronym	no. of dimethyl PEO molecules	no. of dihydroxyl PEO molecules	silica particle	total no. of atoms
peo1	270		no	21 060
peo2		270	no	21 600
peo3	135	135	no	21 330
peosil1	270		yes	22 153
peosil2		270	yes	22 693
peosil3	135	135	yes	22 423

[a] The silica nanoparticle has 1093 atoms.

where r is the distance between atoms i and j, ϵ is the well-depth of the potential, and σ is the distance at which the potential is zero for atoms i and j. The van der Waals parameters corresponding to eq 1 were, as before, derived from the universal force field (UFF).[62] Their consistency with the rest of the potential was checked by carrying out 100 ps MD simulations of crystalline PEO as reported before,[55,63] and it was found that the UFF van der Waals distances[62] had to be slightly decreased to maintain the experimental crystalline density under constant-pressure conditions at 300 K. With σ parameters of 3.0023 Å for (O···O), 3.3150 Å for (C···C), and 2.4553 Å for (H···H) interactions, as well as the standard combination rules of the arithmetic mean for σ and the geometric mean for ϵ, the reparametrized potential was found to keep the PEO crystal density at 1230.8 ±0.2 kg m^{-3}, in close agreement with the experimental value[64] of 1229 kg m^{-3}. The electrostatic potential was evaluated using the Ewald summation method.[65,66]

The parameters for dimethyl PEO were also used for dihydroxyl PEO along with extra interactions related to the presence of the −OH group. The backbone C−O−H bending and C−C−O−H torsional parameters were directly taken from the OPLS united-atom (OPLS−UA) force-field for alcohols.[67,68] In the OPLS−UA force field,[67] there are no explicit 1···4 nonbonded interactions since their effects are taken into account implicitly in the parametrization of the torsion angle potentials. As such, this approach is completely consistent with the one used here, i.e. where equally 1···4 nonbonded interactions are not calculated directly. It thus seemed reasonable to transfer the OPLS−UA torsional potential directly for the C−C−O−H angle.

The charges on the hydroxyl end groups were obtained by performing ab initio calculations on a series of two- to five-monomer PEO structures with *Gaussian98*[69] at the B3LYP/6-31G** level. Partial charges, q_i/e, were extracted by an electrostatic potential (ESP) fitting procedure.[70] They were respectively equal to 0.385 for hydroxyl H, −0.611 for hydroxyl O, 0.1356 for their nearest C neighbor, and 0.0452 for both H carried by that nearest neighbor. All other charges were left unchanged,[55,56] and the chains were neutral.

The composition of the six systems under study is shown in Table 1. To compare the behavior of PEO with or without a silica nanoparticle, three pure PEO melts were built, each containing 270 molecules. The **peo1** system is a dimethyl PEO melt, the **peo2** system is a dihydroxyl PEO melt, and the **peo3** system is an equimolar mixture of both types of PEO. A single-chain sampling procedure, based on pivot Monte Carlo moves for rotatable torsions combined with standard MD to explore the various oscillatory modes of the chains, was used to grow the different chains at 400 K. Although this so-called "hybrid PMC-MD technique"[56,71,72] is not strictly necessary here since the chains were eventually decorrelated in the melt using MD on its own, this allows for uncorrelated starting structures. The chains were then randomly reorientated and distributed in a periodic cubic MD box with side length L chosen to give an initial density of 1000 kg m^{-3}, close to the experimentally estimated value for PEO.[73,74]

The full potential was introduced progressively and each system was first equilibrated under constant-volume *NVT* conditions. In all cases, the time-step used was 1 fs. The systems were then switched to *NpT* conditions, in which the isotropic pressure is maintained at the required value of 1 bar

by loose-coupling with a τ_P of 5 ps[75] and the box is kept cubic. The truncation radius for the Lennard-Jones (eq 1) and the real-space part of the electrostatic potential was set at 9 Å. Long-range corrections to the energy and the pressure were made on the assumption that $g(r) = 1$ beyond the cutoff.[30] Optimum convergence of the total Ewald sum[76] in reasonable time for all three pure systems was obtained using a separation parameter, $\alpha = 0.22$ Å^{-1}, and a reciprocal space cutoff, $K_{max} = 12$. The average temperature was kept close to 400 K by weak coupling to a heat bath [77] with a τ_T of 0.1 ps. The equilibration run was carried out until the density stabilized and the chains were totally decorrelated, i.e. typically on the order of ~1000−2000 ps at 400 K. Production runs at $T \sim 400$ K and $p \sim 1$ bar were then extended up to 1000 ps more, over which configurations were stored every 5 ps and thermodynamic and conformational data every 0.5 ps for post-analyses.

2.2. Silica Nanoparticle. The silica nanoparticle used here is based on the recent work of Brown et al.,[50,51] i.e. a hybrid model consisting of an amorphous core linked to a surface coating of silicon atoms and bridging and nonbridging oxygens as well as silanol hydrogens. This fully atomistic description allows for fine-tuning of the surface thickness and number of OH groups per unit surface area while maintaining the ionic characteristics of the silica core.

The ionic core is modeled using the BKS of Van Beest, Kramer, and Van Santen[78] for pure SiO_2, in which Si and O carry partial charges equal to 2.4*e* and −1.2*e*, respectively. As for PEO, van der Waals parameters had to be reparametrized from the Buckingham to the Lennard-Jones form of the excluded-volume potential (eq 1). Their consistency was checked by carrying out 200 ps MD simulations of crystalline α-quartz: it was found that $\sigma = 1.53$ Å and $\epsilon/k_b = 13\,275.88$ K for Si···O interactions and $\sigma = 2.99$ Å and $\epsilon/k_b = 237.8161$ K for O···O interactions gave a good representation of this structure in the bulk.[50,51] It is worth noting that the BKS model does not have van der Waals interactions for Si···Si, as the charges are sufficiently repulsive,[78] and that the Si···O interaction does not come from any empirical mixing rule.

To mimic the atomistic characteristics of silica surfaces, specific intramolecular and partial charge interactions are added to all atoms being defined as part of the surface: the surface silicons (Si_s), the oxygen atoms bridged between two surface silicons (O_b), the nonbridging oxygens atoms linked to only one surface silicon (O_nb) and the silanols hydrogens (HO_nb) linked to the nonbridging oxygens. Explicit bonds are defined between Si_s−O_b, Si_s−O_nb, Si_s−O and O_nb-HO_nb.[49,79] Some other features of the model cylindrical pore representing amorphous silica developed by Brodka et al.[79] are also taken into account. Indeed, an explicit Si_s−O_nb-HO_nb bond angle, with the equilibrium value of 116°,[79] is introduced and the partial charges for O_b, O_nb and HO_nb are set to the values of −0.629*e*, −0.533*e*, and 0.206*e*, respectively.[79] The partial charge on Si_s is set here at 1.290*e*, very close to 1.283*e*,[79] in order to maintain electrical neutrality of our nanoparticle. For all types of silicons and oxygens, van der Waals interactions are identical to those defined for the core. For the hydrogens, the Brodka model[79] uses the same approach as various water models;[80,81] i.e., their nonbonded interactions are represented by charges only.

The creation of a nanoparticle of radius R_n was carried out in several steps. As it was noticed by trial and error that, in order for the surface layer to form a percolating network, the target surface thickness should be $R_n - 9$ Å,[49] the target particle radius R_n was initially set to the 15−17 Å range. Considering the pure PEO melts, this would amount to silica volume fractions of roughly 6 to 9%. The actual R_n (see later) was related to the target magnitude of silanol number, i.e., a constant $\alpha_{OH} = 4.6$ OH nm^{-2} when the surface is hydroxylated to the maximum degree, as determined by Zhuravlev.[82]

A (39 Å)^3 cubic box of α-quartz consisting of 6561 atoms was first built and simulated at room temperature for 100 ps using the BKS re-parametrized model described above. The truncation radius for the Lennard-Jones and the real-space part of the electrostatic potential was $R_c = 13.5$ Å. The Ewald parameters were respectively $\alpha = 0.30$ Å^{-1} and $K_{max} = 14$. The crystalline structure was found to be well conserved. To "amorphize" such a crystal, the most common approach would be to heat it up. Although this was used elsewhere,[51] it is quite drastic compared to the experimental condensation polymerization of $Si(OH)_4$.[82] As such, we used a softer approach where the nonbonded parameters of the α-quartz MD simulation were modified in order to decrease the interactions between Si and O: with $\alpha = 0.90$ Å^{-1} and $K_{max} = 0$, only the repulsive part of the Lennard-Jones being conserved and the truncation radius R_c set to 5 Å, the extent of amorphization was followed under constant-volume and constant-pressure conditions by monitoring the radial distribution functions. The procedure was deemed to be complete when the only structures remaining were those of a Si surrounded by 4 O atoms. The amorphous silica box was then compressed back to ~2200 kg m^{-3} ,[83] and the full potential was progressively reintroduced. The system relaxed toward a final density of 2380 ± 1 kg m^{-3}.

To create a roughly spherical silica nanoparticle, Si and O atoms outside the R_n target radius from the center of the amorphous silica box were discarded. The initial particle was cut out with exactly twice the number of oxygen atoms than silicons, to remain electrically neutral. It was then relaxed under constant volume *NVT* conditions at 300 K for 1 ps, using the same model than the bulk melt, to enable a rearrangement of the surface zone. This short relaxation phase was found to limit the number of multiple silanols eventually present on the surface. Following the relaxation step, all silicons having less than four near-neighbor oxygens were first removed. The connectivity of the surface layer was progressively defined by an iterative algorithm using 1.9 Å as a bonding criteria. Isolated oxygens, i.e., those having no silicon within 1.9 Å, were eliminated. Subsequently, the oxygens linked to only one near-neighbor silicon became nonbridging or silanol oxygens (O_nb), the silicons linked to these O_nb became surface silicons (Si_s), the oxygens linked to two Si_s became bridging oxygens (O_b) and so on. R_n and the final number of O_nb could then be directly related to the target α_{OH} by adding silanol hydrogens (HO_nb). In this work, the nanoparticle was obtained for an initial value of $R_n = 16.3$ Å, which corresponded to 1093 atoms and a volume fraction of ~8% in the PEO−silica mixtures. Following the surface reorganization, the actual diameter of the particle was closer to ~3.0 nm, and it had an $\alpha_{OH} = 4.4$ OH nm^{-2}, i.e., very close to the Zhuravlev constant.[82] In addition, the different types of silanol groups could be distinguished. Our model nanoparticle had 82% ≡SiOH, 17% ═$Si(OH)_2$ and 1% −$Si(OH)_3$. This is in good agreement with the experimental results which give roughly 87% ≡SiOH and 13% ═$Si(OH)_2$ for $\alpha_{OH} = 4.6$ OH nm^{-2}.[82] It is also worth noting that the nanoparticle obtained in this way has a certain roughness, as should be expected. A schematic representation of the nanoparticle within the dihydroxyl PEO system is shown in Figure 1.

It is worth mentioning that the same type of procedure could be adapted to create a model of a flat silica surface. A slab configuration, such as the PEO/TiO_2 model of Borodin et al.,[53] would certainly increase the amount of surface for a given (cubic) volume of PEO. However, for our hybrid model of amorphous silica, it would also increase the volume of silica that would be needed to be simulated: given that a depth of silica of ~10 Å would be required from each face to model the transition from surface to bulk and to be consistent with a cutoff radius of ~10 Å, this implies a slab of silica of ~20 Å thickness. The ratio of surface area to volume of silica in this geometry is thus only about 0.10, compared to an actual value of 0.22 in the spherical inclusion case.

2.3. PEO—Silica Models. Three **peosil** models corresponding to the pure melts were prepared (Table 1). The **peosil1** system refers to dimethyl PEO−silica, the **peosil2** system refers to dihydroxyl PEO−silica and the **peosil3** system refers to the equimolar mixture of both types of PEO−silica. The technique for merging the nanoparticle with the polymer melt is described in detail elsewhere.[49,54] The polymer box was first expanded, and then a 17 Å-cavity was created in its center using a soft repulsive potential:

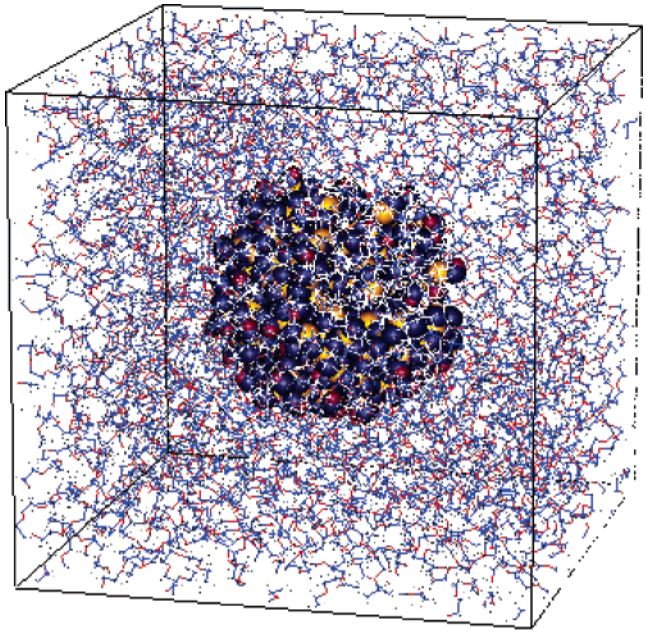

Figure 1. Schematic representation of the hydroxyl-terminated PEO−silica (**peosil2**) simulation box. The polymer and nanoparticle are represented in wire-frame and space-filling models, respectively. For clarity, PEO molecules in the top front right corner have been removed in this display in order to better reveal the nanoparticle.

$$U_{cav}(\mathbf{r}_i) = \frac{1}{2} k_{cav}(|\mathbf{r}_i - \mathbf{R}_0| - r_{cav})^2 \quad \text{for } |\mathbf{r}_i - \mathbf{R}_0| < r_{cav} \quad (2)$$

with k_{cav} being a force constant equal to 50 kg s^{-2}, $\mathbf{r}_i$ the current position vector of polymer atom i, $\mathbf{R}_0$ the center of the MD box, and r_{cav} the current radius of the cavity. The nanoparticle described in section 2.2 was then inserted into the spherical cavity.

For the PEO−silica potentials, in addition to the Coulombic forces, van der Waals interactions between silicons and PEO oxygens used the same parameters than those between silicons and nanoparticle oxygens. All remaining van der Waals cross-terms used Lorentz−Berthelot combination rules.[30] This meant that interactions between the silicons as well as the silanol hydrogens with the PEO carbons and hydrogens were represented by electrostatic contributions only. This kind of approach was used by Brodka et al. to model acetone in a silica pore.[79]

A 10 ps minimization run was first carried out in order to remove high-energy contacts. As for the pure **peo** melts, the **peosil** systems were then switched to constant-pressure *NpT* conditions at 400 K. The truncation radius for the Lennard-Jones (eq 1) and the real-space part of the electrostatic potential was set at 9.5 Å. The Ewald parameters were $\alpha = 0.24$ Å^{-1} and $K_{max} = 12$. All other details were identical to those of the pure melts. The equilibration runs were carried out until the PEO chains were totally decorrelated from their starting structure around the nanoparticle, i.e., typically on the order of 1 or 2 ns at 400 K. Production runs at $T \sim 400$ K and p $\sim$ 1 bar were then extended up to 1000 ps more, and data were stored for post-analysis. A schematic representation of the **peosil2** system is shown in Figure 1.

3. Results and Discussion

3.1. Chain Decorrelation. To prevent artifacts related to the extensive preparation procedures, PEO oligomers in both pure matrix systems and nanocomposites were first decorrelated at 400 K using MD. This is an important point, as the preparation procedure has been shown to be critical in realistic models of PBMA−silica nanocomposites, where the long and relatively stiff polymer chain remained highly correlated to its starting structure.[50,51] In the present work, the chains were chosen to be much shorter and more flexible so that complete decorrelation could occur on the time scale available to standard MD simulations.

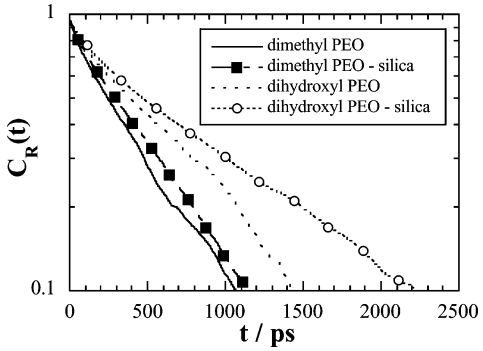

Figure 2. Normalized autocorrelation functions for the square end-to-end distances of PEO chains at 400 K. The $C_R(t)$ values are extracted from the **peo1** and **peosil1** systems for dimethyl chains and from the **peo2** and **peosil2** systems for dihydroxyl chains.

The extent of decorrelation of PEO in a system was monitored using the normalized autocorrelation function for the square end-to-end distances of the chains, $C_R(t)$, averaged over all molecules and over all available time origins. If the square end-to-end distance of a PEO chain at time t is $R^2(t)$, then:

$$C_R(t) = \frac{\langle R^2(0)R^2(t)\rangle - \langle R^2\rangle^2}{\langle R^4\rangle - \langle R^2\rangle^2} \quad (3)$$

$C_R(t)$ will follow configurational relaxation, which is usually much slower than conformational relaxation.[56,72] The characteristic decorrelation time scales for the systems under study are shown in Figure 2. The dimethyl chains (from the **peo1** and **peosil1** systems) decorrelate within ~1 ns, while dihydroxyl chains (from the **peo2** and **peosil2** systems) relax within ~1.5−2.5 ns. Similar results are found in the mixed **peo3** and **peosil3** system. As expected, the silica nanoparticle slows up decorrelation of the surrounding melt, but it is clear from Figure 2 that all systems under study could be fully relaxed in a reasonable time for MD simulations. Their respective decorrelation time scales were used as the start of the production runs. Consequently, all subsequent analyses were carried out on oligomer systems which were independent of their starting structures.

3.2. Volumetric Properties. The global average density of the six systems is given in Table 2 along with the corresponding volumes, pressures and intermolecular energies. As expected, the average pressures $\langle p\rangle$ confirm that all systems remain around ~1 bar.

The densities of the three pure model PEO melts fall within the 1000−1050 kg m^{-3} range. Densities for PEO oligomers of number-averaged molecular weight 400 (~9 monomers) have been experimentally measured in the 300.15 to 328.15 K temperature range.[84] Extrapolating their data up to 400 K predicts a density of ~1041 kg m^{-3}. Other experimental data for similar chains report densities on the order of 1130 kg m^{-3} at 273 K.[85] With a calculated value for the molar thermal expansivity of liquid PEO of 242 × 10^{-4} cm^3 mol^{-1} K^{-1},[74] the corresponding density at 400 K will be ~1048 kg m^{-3}. Both experimental sources are thus in excellent agreement

Table 2. Details of the Simulations Undertaken at 400 K[a]

system	peo1	peosil1	peo2	peosil2	peo3	peosil3
$\langle\rho\rangle$	1004.2	1095.5	1050.1	1139.1	1027.6	1116.1
$\langle V\rangle$	210 100	221 900	214 600	226 000	212 300	224 200
$\langle p\rangle$	2	1	0	3	1	1
$\langle U^{\text{inter}}_{\text{total}}\rangle$	−21.62	−181.83	−23.44	−184.08	−22.61	−182.96
$\langle U^{\text{inter}}_{\text{total silica−silica}}\rangle$		−158.65		−158.74		−158.66
$\langle U^{\text{inter}}_{\text{total PEO−PEO}}\rangle$	−21.62	−21.14	−23.44	−22.93	−22.61	−22.07
$\langle U^{\text{inter}}_{\text{total PEO−silica}}\rangle$		−2.04		−2.41		−2.23
$\langle U^{\text{inter}}_{\text{LJ}}\rangle$	−19.24	−26.22	−19.54	−26.67	−19.49	−26.51
$\langle U^{\text{inter}}_{\text{LJ silica−silica}}\rangle$		−5.65		−5.65		−5.67
$\langle U^{\text{inter}}_{\text{LJ PEO−PEO}}\rangle$	−19.24	−18.82	−19.54	−19.16	−19.49	−19.05
$\langle U^{\text{inter}}_{\text{LJ PEO−silica}}\rangle$		−1.75		−1.86		−1.79
$\langle U^{\text{inter}}_{\text{ele}}\rangle$	−2.38	−155.61	−3.90	−157.41	−3.12	−156.45
$\langle U^{\text{inter}}_{\text{ele silica−silica}}\rangle$		−153.00		−153.09		−152.99
$\langle U^{\text{inter}}_{\text{ele PEO−PEO}}\rangle$	−2.38	−2.32	−3.90	−3.77	−3.12	−3.02
$\langle U^{\text{inter}}_{\text{ele PEO−silica}}\rangle$		−0.29		−0.55		−0.44

[a] The average densities $\langle\rho\rangle$ are given in kg m^{-3} with a maximum standard error of ± 0.5 kg m^{-3}. $\langle V\rangle$ are the average volumes of the MD cells in Å^3 with a maximum standard error of ± 50 Å^3. The average pressure $\langle p\rangle$ is in bars with a maximum standard error of ±4 bar. The average intermolecular potential energies $\langle U\rangle$ are all quoted in kJ per mole of PEO monomer with a maximum standard error of ±0.03 kJ mol^{-1} mon^{-1}. $\langle U^{\text{inter}}_{\text{total}}\rangle$ are the total intermolecular energies, while $\langle U^{\text{inter}}_{\text{LJ}}\rangle$ and $\langle U^{\text{inter}}_{\text{ele}}\rangle$ are the total Lennard-Jones and electrostatic contributions to the intermolecular energies, respectively. Also shown for the PEO−silica systems are the specific contributions of silica−silica, PEO−PEO and PEO−silica interactions to the aforementionned intermolecular energies.

with the dihydroxyl **peo2** density. Although we are not aware of density−temperature data on short dimethyl **peo1** oligomers, the same model used for longer chains has also been shown to agree with experimental and empirical results.[56,57] The **peo1** and **peo2** simulations can thus be considered as being well representative of the real systems. It should be mentioned that, as shown by the simulation box volumes, the lower density for dimethyl PEO is not related to an expansion of the system with respect to dihydroxyl PEO. It is simply due to an over-compensation in the **peo2** density of the extra mass of hydroxyl oxygens with respect to the increase of volume. The **peo3** model volumetric properties are close to the exact averages between **peo1** and **peo2**. Indeed, both types of chains are similar enough to form an almost ideal mixture as they only differ by their end groups.

Inserting a nanoparticle in the pure melt leads to a systematic increase in density by ∼8.5−9%. The respective simulation boxes are found to expand by 11800 Å^3 for **peo1**, 11400 Å^3 for **peo2**, and 11900 Å^3 for **peo3**. If the oligomer−filler mixtures were ideal, this would correspond to a nanoparticle of average radius ∼14 Å. To estimate the actual volume of our silica nanoparticle, we used a simple Monte Carlo procedure in which probes of a preset radius are randomly and independently inserted into the silica MD box (section 2.2). The nanoparticle atoms were represented by hard spheres with standard van der Waals radii as determined by Bondi.[74] A total of 500000 trial insertions were attempted for probes radii ranging from 0 to 2.5 Å, and only those probes which did not overlap with the hard spheres were accepted. A breaking point in the insertion acceptance rate vs probe radius curve was found for 0.62 Å, which basically corresponded to the upper limit size for a probe to be inserted into the nanoparticle. By subtraction of this probe-accessible volume from the total volume of the MD box, the volume of our nanoparticle could be estimated at ∼14665 Å^3, i.e., an average radius of ∼15.2 Å and a volume fraction of ∼6.5%. As shown later, this result is consistent with other analyses. Since this estimation is significantly larger than the expansion of the pure melts, it is clear that the net interactions between silica and PEO will be attractive, thus leading to a reduction of the expected volume expansion.

To further analyze the effect of the nanoparticle on the density, the radial mass density $\rho(R)$ of the polymer chains as a function of the distance R from the center-of-mass of the nanoparticle was calculated. $\rho(R)$ is given in Figure 3a for the dihydroxyl **peosil2** system, with the total contribution of the polymer chains as well as the specific profiles of the backbone oxygens and carbons. For comparison, the mass density of the silica particle is also displayed. It confirms that ∼15.2 Å is a good value for the nanoparticle radius. It should be noted that another way to estimate the effective nanoparticle radius is to associate it with the separation at half-maximum of the first peak in the pair distribution function (equivalent to the mass density function shown in Figure 3a), as has been done by Smith et al.[45] However, these authors determined their filler radius on a coarse-grained system with neutral nanoparticle−polymer interactions and a well-defined sharp first peak.[45] In our systems, the first peak is much smoother and this approach overestimates the particle radius.

As reported by other coarse-grained and realistic simulations,[35,36,40,43,45,46,49,50,53] Figure 3a shows that the PEO molecules close to the interface are arranged in densely packed shells and that, at larger distances, the mass density eventually tends toward the average density of the pure melt. There are two distinct maxima at ∼17.0 and ∼21.5 Å from the nanoparticle center-of-mass and a third less-precise maxima at ∼26.0 Å of intensity decreasing with increasing R. Layering is known to be directly related to the nature of polymer−surface interactions, i.e. well-defined for strongly attractive systems and much less-defined at interfaces with weaker polymer−surface interactions.[43,46,53] It is interesting to note that, although structuring is visible, it is less clear than for generic models,[35,36,40,43] as had already been noted when comparing a generic united-

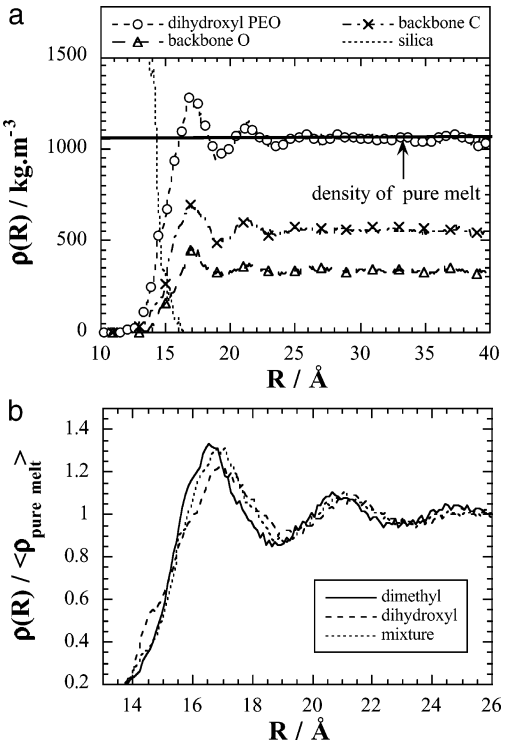

Figure 3. Radial mass density as a function of the distance R from the center-of-mass of the silica particle for (a) contributions of all the dihydroxyl PEO atoms, the PEO backbone oxygens, the PEO backbone carbons, and silica in the **peosil2** system and (b) the dimethyl (**peosil1**), dihydroxyl (**peosil2**), and the equimolar mixture of both PEO (**peosil3**) systems. In part b, the $\rho(R)$ curves have been normalized with respect to the average densities of their respective pure melts.

atom CH_2 to a fully atomistic PBMA model.[49,50] As expected, the higher mass-densities are found for those oligomers which are at the immediate vicinity of the particle, but the silica surface is rough and some parts of the flexible PEO molecules can even access the coverage which is not shielded by silanol oxygens. Borodin et al. also identified three layers in their PEO density profile in the vicinity of their TiO_2 flat surfaces,[53] which would suggest that the PEO structuring is not specifically related to the spherical geometry of the filler. However, they reported an alternating positioning of the carbon atoms between two layers of oxygen atoms in their first layer,[53] a feature which seems to be related to the rigid crystalline nature of their TiO_2 surface. In the present case, this is not seen in Figure 3a and is probably due to the roughness of our amorphous silica surface. The influence of our nanoparticle on our dihydroxyl PEO oligomers spans the approximate range of R from 13 to 28 Å, i.e., a total of ∼15 Å. As the center-of-mass of the closest neighboring nanoparticle via the periodic boundary conditions is situated at more than 60 Å, this structuring is solely dependent on the main particle under study.

The $\rho(R)$ of the different PEO oligomers, normalized with respect to the density of their corresponding pure melt, are all shown together in Figure 3b. Differences between the three systems can only be found for the first layer, which extends over ∼5 Å. There is a shoulder between 14 and 15 Å which is characteristic of dihydroxyl PEO. This feature is attenuated in the equimolar PEO mixture. In dimethyl PEO the first peak is slightly shifted to lower R. The equimolar mixture always has an intermediate behavior. These changes will be related to the structural influence of the end groups at the immediate vicinity of the nanoparticle (see later). On the other hand, the second peak, from 19 to 23 Å, is very similar for all three PEO. The influence of the end groups thus seems much less distinct when they are further away from the nanoparticle. Unlike generic models,[35,36,40,43,49] there is a lack of fixed periodicity in the layer widths, but it seems to be an artifact mostly related to the inhomogeneity of the particle surface, which only directly affects the first layer. The third layer is harder to distinguish from the melt, but also extends over ∼4 Å.

3.3. Intermolecular Energies. The average intermolecular energies, quoted in kJ per mole of PEO monomer, can also be found in Table 2. The average total intermolecular energies $\langle U_{total}^{inter} \rangle$ have been resolved into their van der Waals $\langle U_{LJ}^{inter} \rangle$ and their electrostatic $\langle U_{ele}^{inter} \rangle$ components for each specific contribution, i.e the separate silica−silica, PEO−PEO and PEO−silica interactions.

In the pure **peo1**, **peo2**, and **peo3** melts, the excluded-volume van der Waals interactions amount to 80−90% of the total intermolecular PEO−PEO energy. The addition of hydroxyl groups slightly stabilizes the **peo2** oligomers, mostly through the extra electrostatic interactions. Similarly to the volumetric properties, the equimolar **peo3** system falls close to the average of **peo1** and **peo2**. As could be expected from its nature, the silica−silica energy is almost totally electrostatic and remains similar in all PEO−silica systems. On the other hand, the PEO−PEO energy is found to decrease when inserting the nanoparticle. This is compensated for by the added PEO−silica attractions. The global behavior of such a system will thus be closer to the attractive interactions case of Starr et al. [42,43] or Smith et al.[45] The nature of PEO−silica interactions is still about 80% excluded-volume and 20% electrostatic, which agrees with the experimental results on the adsorption in PEO−silica occurring through hydrogen bonds.[3−5] Indeed, hydrogens bonds are obtained in these simulations by a combination of van der Waals and electrostatic potentials, and this will be confirmed by the structural analyses. The effect of hydroxyl end groups[14,19,20,27] is reflected in the resulting electrostatic PEO−silica interactions, which are almost doubled with respect to the dimethyl counterparts and thus suggest specific features for this end group at the immediate interface.

We have estimated the change in enthalpy associated with mixing PEO and silica, ΔH, to $\Delta U_{PEO-silica}$ minus the sum of $\Delta U_{pure-PEO}$ and $\Delta U_{nanoparticle}$. The $P\Delta V$ term was found to be less than −0.08 J mol^{-1} mon^{-1} for all three systems under study, and thus negligible in comparison. The corresponding ΔH are −1.56 kJ mol^{-1} mon^{-1} for **peosil1**, −1.90 kJ mol^{-1} mon^{-1} for **peosil2**, and −1.69 kJ mol^{-1} mon^{-1} for **peosil3**. The integral enthalpy of displacement of water by PEO (referring to the enthalpy variation of 1 mol adsorbed from zero coverage up to full coverage) of average molecular weight 400 was found by microcalorimetry to be around −1.5 to −1.8 kJ mol^{-1} mon^{-1} at 298 K and pH 5.5 with experimental uncertainities of ±5%,[14] which is in very good agreement with our model results. This provides some verification of the parameters used for the PEO−silica interactions. For all three cases, the simulations thus enthalpically do predict a favorable mixture of PEO

Table 3. Mean Square Radii of Gyration, $\langle S^2 \rangle$, Percentage of Trans Conformers for the Backbone and End Torsion Angles and Backbone Torsional Relaxation Times for the PEO Chains in the Six Systems Simulated[a]

system	peo1	peosil1	peo2	peosil2	peo3	peosil3
$\langle S^2 \rangle$/Å^2	47.0(1)	45.7(2)	46.7(2)	46.5(2)	48.4(2) 48.8(2)	46.3(2) 46.9(3)
C−O−C−C ⟨% trans⟩	78.5(1)	78.2(1)	79.5(1)	79.2(1)	79.2(1)	78.9(2)
C−O−C−CH_3 ⟨% trans⟩	80.6(1)	80.1(1)			80.7(2)	80.4(3)
O−C−C−O ⟨% trans⟩	11.5(1)	11.3(1)	10.1(1)	10.3(1)	10.9(1)	10.9(1)
O−C−C−OH ⟨% trans⟩			0.29(1)	0.33(2)	0.33(3)	0.29(3)
C−C−O−H ⟨% trans⟩			10.5(1)	11.0(2)	10.0(2)	10.6(3)
C−O−C−C τ_{TT}/ps	11.9(2)	20(1)	15.3(4)	24(2)	17(2) *13.5(3)*	18.5(7) *22(1)*
O−C−C−O τ_{GG}/ps	171(2)	232(2)	251(3)	320(4)	212(3) *209(3)*	251(3) *241(3)*

[a] The two $\langle S^2 \rangle$ values for **peo3** and **peosil3** refer to the dimethyl and dihydroxyl chains, respectively. The relaxation times in italics are the values obtained assuming the mixtures are ideal. Figures in parentheses indicate the standard error in last digit.

and silica. From the behavior of the cohesive energies, it might be reasonable to assume that the entropy of the chains decreases in the PEO−silica systems, at least close to the interface, thus giving a positive ($-T\Delta S$) contribution to the free energy ΔG and partly counteracting the negative ΔH term. However, the mere fact that PEO is known experimentally to adsorb on silica from solutions[9] suggests that the entropic term is relatively small with respect to the enthalpic term, leading to a negative ΔG for these PEO−silica mixtures.

3.4. Chain Configurations and Conformations. The PEO oligomer configurations can be characterized by their mean square radii of gyration, $\langle S^2 \rangle$. These are given in Table 3, along with the mean values for the percentage of trans conformers for PEO backbone and specific end-torsions. Please note that we use the dihedral angle convention where τ is *gauche*$^-$ (G^-) if $-180° \leq \tau \leq -60°$, trans (T) if $-60° < \tau < 60°$, and *gauche*$^+$ (G^+) if $60° \leq \tau \leq 180°$.

All $\langle S^2 \rangle$ values fall within the 47−49 Å^2 range, which corresponds to an average radii of gyration of ∼6.8−7 Å. They are thus significantly smaller than the silica nanoparticle radius, which, according to in vacuo MD results,[10] should promote a relatively saturated surface.

As far as conformational properties are concerned, the backbone O−C−C−O ⟨% trans⟩ reflect the well-known gauche effect in PEO, i.e., the fact that torsions around C−C bonds are mainly found in the gauche state, while the C−O−C−C angles tend to favor the trans state.[56,86,87] The C−O−C−CH_3 and O−C−C−OH end-torsions behave similarly to their backbone analogues, except that their populations in the lowest energy wells increase. There is a slight increase in ⟨% trans⟩ for the methyl end-torsions C−O−C−CH_3 related to the steric effect of the −CH_3 group, while the O−C−C−OH and C−C−O−H end-torsions are now almost totally in the gauche state, because of the combined electrostatic and steric influences of the −OH group. Interestingly, plotting the values of O−C−C−OH angles vs their neighboring C−C−O−H angles reveals that these successive angles are mostly found in approximately equal proportions either in G^+G^- or in G^-G^+ states. This feature is independent of the presence of the nanoparticle and is related to a strongly favored intramolecular 1···5 interaction between the hydroxyl H and the first backbone O ether in dihydroxyl PEO. Indeed, a well-defined peak can be found at ∼2.40 Å in the corresponding intramolecular radial distribution functions. These variations will in turn affect the nearest backbone torsions; hence, small differences are observed between dimethyl and dihydroxyl PEO.

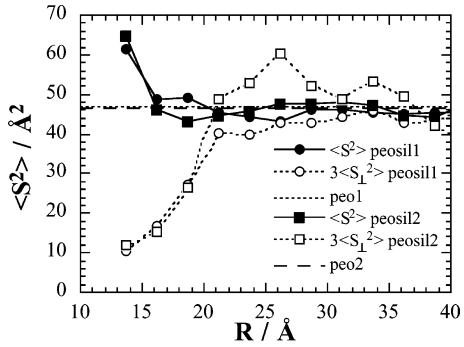

Figure 4. Mean square radii of gyration as a function of the distance R from the center-of-mass of the silica particle for the **peosil1** and **peosil2** simulations. The total (filled symbols) and the component perpendicular to the nanoparticle surface multiplied by three (open symbols) are given. The histograms are accumulated using the distance from the center-of-mass of each chain to the center-of-mass of the nanoparticle using a resolution of 2.5 Å. The dotted and dashed horizontal lines give the average values for the corresponding pure melts.

It is clear from Table 3 that neither the end groups nor the presence of the nanoparticle have a large effect on the *average* conformational and configurational properties of the PEO oligomers. The fact that the overall chain dimensions are largely independent of the presence of the nanoparticle has already been noted in other simulations,[42,43,45,49,51] although Vacatello did report, as can be found in Table 3, a moderate decrease of a few percent in radii of gyration in his Monte Carlo calculations of dense polymer melts filled with solid nanoparticles.[35−37] On the other hand, we would expect the conformation of the molecules to be at least distorted close to the interface and partly dependent on the end groups. This is corroborated by experimental evidence suggesting conformational changes for short hydroxyl-terminated PEO.[14,19,20,27]

To spatially resolve the possible changes in the configurations and conformations, the square radius of gyration and the % trans of torsional angles have also been calculated as a function of the distance R from the center-of-mass of the nanoparticle. Figure 4 presents the results for the radial dependence of the mean square radii gyration for the **peosil1** and **peosil2** systems. Similar results, not shown, were obtained for the equimolar mixture. The behavior of $\langle S^2 \rangle$ with R suggests that only right at the interface itself is there a strong effect on chain configurations with a tendency toward elongation. However, resolving $\langle S^2 \rangle$ into components perpendicular, $\langle S_\perp{}^2 \rangle$, and parallel to the interface reveals that this is not the full story. The variation of $\langle S_\perp{}^2 \rangle$ with

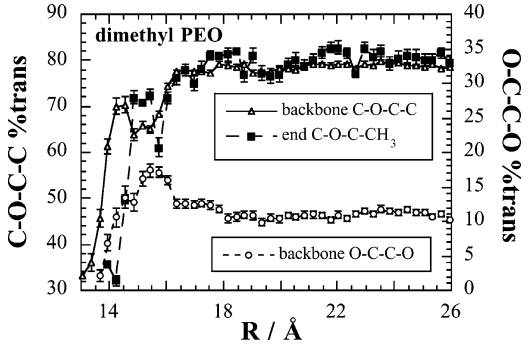

Figure 5. Mean percentage of trans conformers for the dimethyl **peosil1** backbone and end group torsional angles as a function of R. The resolution is 0.3 Å, and torsions are assigned to a bin according to the value of R for the position of the second atom in the torsion. Standard errors are at the most a few percent. Note that these plots are double-Y with C−O−C−C torsions on one side and O−C−C−O torsions on the other side.

R, also plotted in Figure 4, shows that the chains are "flattened" against the nanoparticle surface and that this happens for a range corresponding to at least the width of the first layer. Similar findings have been reported previously for model nanoparticle systems,[42,43] and the same relative order of reduction in $\langle S_\perp{}^2 \rangle$ has been found in the case of PEO chains close to a planar TiO_2 surface even though a higher degree of polymerization (DP = 54) was used.[53] Clearly the parallel component increases in a way which compensates for the diminution of the perpendicular one except right at the interface where it exceeds it sufficiently to cause an overall increase in $\langle S^2 \rangle$.

Results for the % trans vs R are shown in Figure 5 for the dimethyl **peosil1** system but are similar for the **peosil2** and to a lesser extent the **peosil3** simulations. There are indeed variations but they only span the first PEO layer before returning to their pure melt values (see Table 3). The backbone C−O−C−C torsions in the first layer of the silica interface have a tendency to adopt more gauche conformations than in the melt, thus explaining the slight decrease in the overall averages for silica-containing systems. An increase in the probability of gauche conformations restricted to the first layer has also been reported in the case of PEO chains at a crystalline TiO_2 interface.[53] These adjustments in the flexible backbone of such oligomers indicate that effective surface coverage is not only related to end groups. The backbone O−C−C−O torsions also tend to be more in gauche states very close to the interface but then there is a rapid rise toward a peak in the first layer where the trans state is about 5% more probable than the mean in the pure melt (see Figure 5). This profile effectively cancels out any net change in the overall O−C−C−O trans population, as can be seen from Table 3. As far as the chain ends are concerned, the hydroxyl end always remains in their gauche conformations (results not displayed), whereas the methyl groups are sensitive to the presence of silica: the C−O−C−CH_3 end angles adopt more gauche conformations in the immediate vicinity of the filler for steric reasons.

It is worth noting that these effects are contrary to the generic model of a polymer matrix and a pure silica nanoparticle of Brown et al. where the % trans was increased out to a range of at least 40 Å.[49] In this particular case, the flexibility of the polymer allowed it to accommodate the initial insertion of the nanoparticle, but afterward the long relaxation times prevented the polymer from attaining equilibrium. In the fully atomistic model of PBMA−silica, the polymer was too rigid to adapt to the inclusion and the % trans remained basically the same.[50,51] In the present work, the chains are short and flexible and have time to come to equilibrium adopting a specific structure. As will be shown later, there are a lot of end groups at the surface, which compete with the backbone fragments.

3.5. Alignment. The structural variations can also be studied in terms of the degree of alignment of the chains with respect to the interface as a function of R. We used the same type of approach as Vacatello [35] and Brown,[49] and calculated the first two Legendre functions, $P_1(\cos\theta)$ and $P_2(\cos\theta)$, where θ for a backbone or end group triplet of atoms $\{i, j, k\}$ is defined as the angle between the vector from the center of mass of the nanoparticle to atom j and the vector between atoms i and k. $P_1(\cos\theta)$ and $P_2(\cos\theta)$ are given by

$$P_1(\cos\theta) = \langle \cos\theta \rangle \tag{4}$$

$$P_2(\cos\theta) = \frac{3}{2}\langle \cos^2\theta \rangle - \frac{1}{2} \tag{5}$$

Both Legendre functions were calculated for specific backbone or end group types. $P_1(\cos\theta)$ should be zero for all values of R because of the symmetry and was only used here as a consistency check to assess the statistical significance of the results for the lowest and highest values of R. Those points with manifestly nonzero values for $P_1(\cos\theta)$ were excluded but this amounted to less than 0.5% of the total number of angles. $P_2(\cos\theta)$ as a function of R were obtained with a resolution of 0.5 Å for backbone torsions, and with a resolution of 1.5 Å for the fewer end-torsions.

$P_2(\cos\theta)$ will indicate the preferential alignments as its limiting values are $-1/2$ for a perfectly perpendicular alignment, 1 for a perfectly parallel alignment, and 0 for a random alignment of the vectors defining θ. Figure 6a displays the combined backbone O−C−C and C−O−C $P_2(\cos\theta)$ for the dimethyl **peosil1** system; very similar results were obtained for the other systems. If this function is compared to the corresponding mass density curve (see Figure 6a), a clear correspondence with the PEO layers can immediately be noticed. Indeed, the alignment is random in trough regions of $\rho(R)$, while there is a tendency toward perpendicular alignment with respect to the outward pointing normal to the interface, i.e., a parallel alignment of these backbones angles with respect to the silica surface in high-density regions. This effect is strongest for the first layer and obviously favors packing. It is in broad agreement with the alignment observed by other simulation work in the vicinity of a surface.[35,49,88] Interestingly, the range of the alignment effect for our detailed model of a PEO oligomer liquid, two or three molecular layers, is also intermediate between that found for the liquid generic oligomer system of Vacatello[35] and the solid long chain polymer model of Brown et al.[49]

Figure 6b compares the alignment of methyl-terminated and hydroxyl-terminated angles in the **peosil3** equimolar mixture. A similar behavior is found in the pure PEO−silica systems. The methyl-terminated angles tend toward parallel alignments with respect to the silica surface whereas the hydroxyl-terminated angles are more perpendicular to the surface. The model appears to reproduce the experimental conclusion that

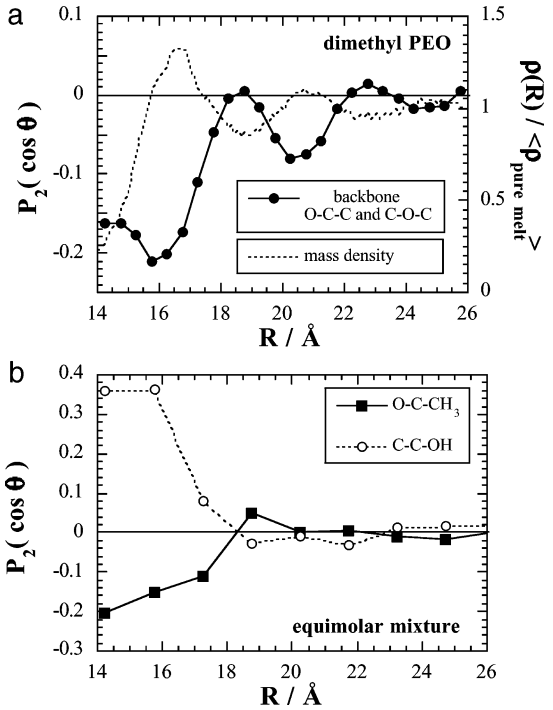

Figure 6. Mean values of $P_2(\cos\theta)$ as a function of R. Part a shows the total contribution of the O−C−C and C−O−C backbone angles to P_2 with a resolution of 0.5 Å in the dimethyl (**peosil1**) system compared to its mass density. Part b shows the effect of the end group angles in the equimolar mixture of both PEO (**peosil3**) with a resolution of 1.5 Å.

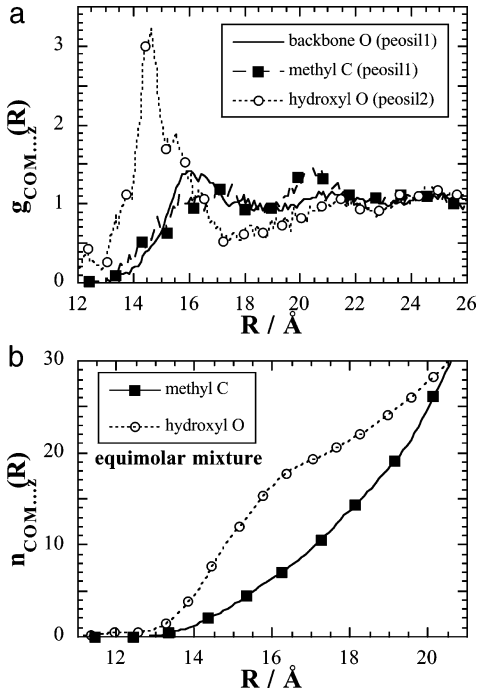

Figure 7. (a) Radial distribution functions, $g_{COM...z}(R)$, for atoms of type z situated at a distance R from the center-of-mass and (b) the average total number of atoms of type z found at a distance R from the center-of-mass, $n_{COM...z}(R)$. Part a shows the end group contributions to $g_{COM...z}(R)$ in both dimethyl (**peosil1**) and dihydroxyl (**peosil2**) systems along with the backbone oxygen $g_{COM...z}(R)$ for **peosil1**. Part b gives the average number of end group atoms as a function of R in the equimolar mixture of both PEO (**peosil3**).

hydroxyl end groups allow the PEO molecules to partially "stand up" with respect to the silica surface at maximum adsorptions, which has been suggested to interpret its specific double-plateau adsorption isotherm.[14,19,20,27]

3.6. Radial Distributions Functions. Structural features were also analyzed using the radial distribution functions, $g(r)$, which can readily be calculated from the atomic coordinates.[30] The typical backbone-backbone $g(r)$ functions corresponding to our PEO bulk melt have already been presented elsewhere.[57] If we compare the filled and unfilled systems, we find the same features than for the chain dimensions, i.e., that there is no obvious difference in the backbone−backbone PEO curves. This has been observed by Starr et al.,[43] who suggested that the structural effect of the monomers close to the surface was overwhelmed by the rest of the melt.

However, radial distribution functions, such as the $g_{COM...z}(R)$ between the nanoparticle center-of-mass (COM) and a given atom type z, can also be characterized as a function of R. Some typical $g_{COM...z}(R)$ values are displayed in Figure 7a. These curves are well representative of all three PEO−silica systems. In the same way as in Figure 6a, the backbone atoms $g_{COM...z}(R)$ correspond almost exactly to the PEO layers; i.e., their maxima and minima fall in the high- and low-density regions, respectively. The methyl carbons $g_{COM...z}(R)$ are hardly differentiated from the backbone carbons, which suggests that there is little specific affinity for this end group on the silica surface. On the contrary, the hydroxyl oxygens $g_{COM...z}(R)$ exhibit a very strong peak, which is obviously related to specific interactions between the surface and these end groups in both **peosil2** and **peosil3** systems. This peak can be associated with the small shoulder around $R\sim14-15$ Å seen in the $\rho(R)$ of dihydroxyl PEO−silica (see Figure 3b). The $g_{COM...z}(R)$ curves were integrated to give the total number of atoms of type z within a radius R of the silica center-of-mass, $n_{COM...z}(R)$:

$$n_{COM...z}(R) = 4\pi \frac{N_z}{\langle V\rangle} \int_0^R g_{COM...z}(s) s^2 \, ds \qquad (6)$$

where N_z is the total number of atoms of type z in the system, and $\langle V\rangle$ is the average volume of the simulation box. Despite the same number of methyl-terminated and hydroxyl-terminated molecules in the equimolar PEO mixture (**peosil3**) system, Figure 7b reveals that there are clearly far more hydroxyl end groups in the vicinity of the nanoparticle than their methyl counterparts. The closer to the particle surface, the more pronounced the relative affinity for hydroxyl end groups is: for example, at $R = 15$ Å, there will be on average ∼11.6 −OH ends for ∼3.6 $-CH_3$ ends, which amounts to an $-OH/-CH_3$ ratio of ∼3.2. The $-OH/-CH_3$ ratio becomes ∼2.6 at $R = 16$ Å, ∼2.0 at $R = 17$ Å, ∼1.5 at $R = 18$ Å, and ∼1.3 at $R = 19$ Å and is only equal to ∼1 for $R = 20.6$ Å. The shoulder in the hydroxyl O curve of Figure 7b corresponds to the end of the main structural peak found in Figure 7a. As most −OH groups are close to the filler, there will be more remaining $-CH_3$ groups in the rest of the melt, which is reflected in the $n_{COM...z}(R)$ curves for larger R values.

The $g(r)$ and $n(r)$ functions were also calculated for specific pairs of PEO vs nanoparticle atom types. As expected, the closest peaks in the $g(r)$ functions are found for interactions between PEO atoms and silanol hydrogens or oxygens. They are shown in Figure 8.

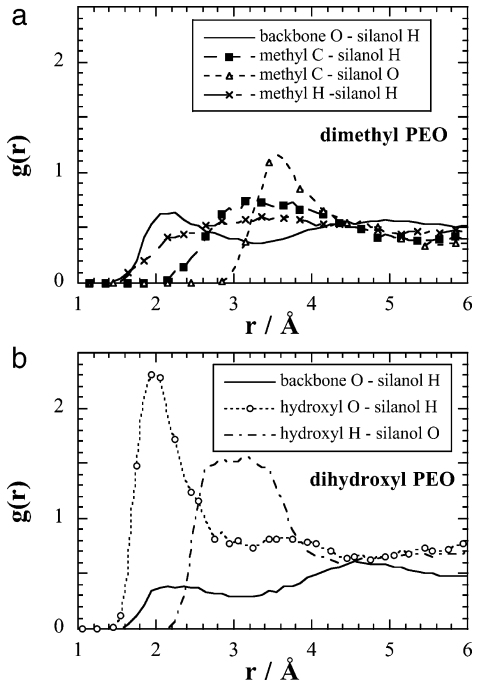

Figure 8. Radial distributions functions $g(r)$ between silica atoms and PEO atoms as a function of their distances r. Part a shows the main structures at the dimethyl PEO−silica interface (**peosil1**), and part b shows the main structures at the dihydroxyl PEO−silica interface (**peosil2**).

Figure 8a displays the limited structuring ($g(r) < 1$) of methyl-terminated PEO at the interface. The nearest interactions are those of backbone oxygens with the silanol hydrogens, i.e. the first smooth peak around 2 Å, which corresponds to hydrogen bonding. For steric reasons, the $-CH_3$ groups will not get as deep into the surface, although the small H are able to come in fairly close contact to the silanol hydrogens. This is explained by the only major peak found in these systems representing preferential interactions between the negatively charged silanol oxygens and the positively charged methyl carbon at about 3.6 Å. This is relevant with respect to SFG vibrational spectroscopy experiments, which only detected weak signals using methyl-terminated PEO with fused silica, and concluded that either the chains have a random structure or the CH_2 and CH_3 groups lie down at the interface.[28] Our simulations would suggest the latter as being more probable, although the actual structuring remains fairly weak.

On the other hand, hydroxyl-terminated PEO at the interface is far more structured as can be seen in Figure 8b. It is clear that the main interactions involve the hydroxyl oxygens with the silanol hydrogens, thus confirming their major role at the PEO−silica interface.[3−5] The distance range of the first peak can be related to well-defined hydrogen bonding, with the trough of the radial distribution function (2.8 Å) being considered as the upper limit for the formation of such bonds. The backbone O play much less of a role in the total hydrogen-bonding capability of dihydroxyl PEO, despite the fact that they are five times more numerous than the end groups. Indeed the ratio between the average-number of hydroxyl O around a silanol hydrogen and the average-number of backbone O around a silanol hydrogen goes from 3.5 to 1 over the first peak of Figure 8b. Another interesting feature is that the peak related to the interactions between the hydroxyl H and silanol O is much smoother and found at larger distances than the hydroxyl O−silanol H peak. Hydroxyl H and silanol O are thus prevented from forming hydrogen bonds by the latter interactions, which are more attractive because of their partial charges. This results in the hydroxyl H being pushed away from the surface with respect to the hydroxyl O. The overall picture that emerges can now explain the slight differences seen in the $\rho(R)$ curves of Figure 3b. Indeed, the −OH groups, which form the silanol H−hydroxyl O interaction and the small shoulder characteristic of dihydroxyl PEO, have a tendency to push away not only the hydroxyl H but also the rest of the chains. Its structuring effect is also reflected in the $C_R(t)$ curves (Figure 2), where the slowest decorrelation is exhibited by the dihydroxyl PEO−silica system.

Table 4. Percentages of Average Residence Times for Hydrogen-Bonding Complexes Formed by Hydroxyl O and Silanol H at the Interface[a]

	silanol H involved in		hydroxyl O involved in			
t/ps	1 H bond	2 H bonds	1 H bond	2 H bonds	3 H bonds	4 H bonds
<5	58	89	66	75	82	100
5−10	18	7	17	16	13	
10−15	9	3	7	4	2	
15−20	5		4	2	3	
20−25	3	1	2	1		
25−30	2		1	1		
>30	5		3	1		

[a] Results for **peosil2** and **peosil3** are averaged together.

To further examine the strong hydrogen-bonding structure displayed in Figure 8b, all silanol H and hydroxyl O moieties involved in that first peak were identified over each configuration of the MD production runs. The total number of hydrogen bonds involving silanol H was actually found to fluctuate over time between 22 and 41 with an average of 31.7 for the **peosil2** system. The corresponding numbers were a minimum of 10, a maximum of 23 and an average of 16.6 for the equimolar **peosil3** system. Although these averages correspond to an equilibrium surface coverage well under the total number of silanol H moieties in the nanoparticle under study (124), the underlying dynamics are much more complicated with many different silanol H moieties visited, and in several cases, temporary multiplicity.

The complexity of hydrogen-bond dynamics is illustrated in Table 4. Over time, a specific silanol H can be linked to one (97% of the cases) or two (3% of the cases) hydroxyl O. On the other hand, a specific hydroxyl O can potentially coordinate one (68% of the cases), two (27% of the cases), three (4% of the cases) or even four silanol H (1% of the cases) at the same time. Table 4 provides the respective average residence times for these interactions. The most stable complexes are those where a single silanol H and a single hydroxyl O are bonded together. As soon as the multiplicity increases, steric repulsions become more important and complexes are very short-lived, i.e., < 5 ps for most of them, although they are able to re-form fairly fast. As can be expected, the simultaneous coordination between a hydroxyl O and three or four silanol H often involves geminal $=Si(OH)_2$ groups on the silica surface. However, they can also occur with single-bonded ≡SiOH groups, thus suggesting that those interactions are more dependent on where the silanol H moieties are situated rather than on which surface silicon they are bonded to. Indeed, most of interactions between hydroxyl O and

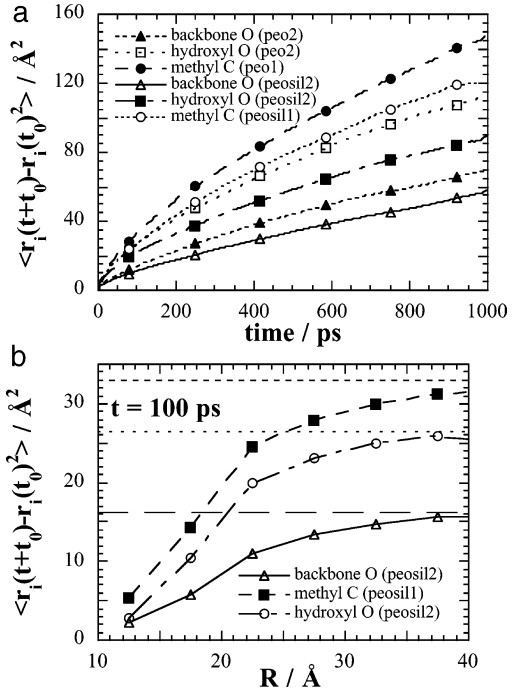

Figure 9. (a) Mean-square displacements (MSDs) of several PEO atom types over the nanosecond production time, averaged over all time origins separated by 5 ps. For comparison, MSDs extracted from both unfilled and filled melts are displayed. (b) MSDs as a function of R at 100 ps intervals. The histograms of interval width equal to 5 Å have been accumulated over all atoms of a given type in a concentric shell and over all time origins. The average MSDs found in the respective pure bulk melt systems are indicated by straight lines.

two silanol H are actually formed with the latter being bonded to different surface silicon atoms. Over the nanosecond time scale of the **peosil2** MD runs simulation, about 75% silanol H moieties were visited by the −OH end groups of the PEO oligomers. This number was only reduced to 57% in the case of the equimolar mixture **peosil3** nanosecond MD run, which confirms the higher affinity of the −OH groups for the silica surface with respect to dimethylated molecules. The molecules were able to form loops, as both −OH ends of a PEO oligomer could be found in the coordination sphere of the same silanol H, albeit very rarely at the same time. The main structural peak displayed in Figure 8b is thus underlined by strong dynamical changes.

3.7. Translational Dynamics. Mean-square displacements (MSDs), corresponding to $\langle (r_i(t + t_0) - r_i(t_0))^2 \rangle$ where the angle brackets imply an average over all atoms of a given type and all possible time origins, t_0, were calculated for each pure PEO and PEO−silica system under study. They were then used to evaluate diffusion coefficients in MD simulations using Einstein's equation:

$$D = \lim_{t \to \infty} \frac{1}{6t} \langle \{r_i(t + t_0) - r_i(t_0)\}^2 \rangle \qquad (7)$$

Some typical MSDs are displayed in Figure 9a in order to establish the influence of the filler on the mobility. The results shown here come from the **peo1**, **peosil1**, **peo2**, and **peosil2** systems, which have better statistics for the end groups, but they are also well representative of the equimolar mixture simulations. In the PEO−silica systems, the nanoparticle atoms remain close to their initial positions with MSDs less than 2−3 Å^2. On the other hand, the oligomer MSDs are much closer to their values in the pure melt; i.e. they indicate diffusion up to ∼1 nm in 1 ns. Despite the relatively high temperature (400 K), the production time is still too limited to reach the Einstein limit, i.e., the region where MSDs are truly linearly proportional to t. Indeed, double logarithmic (MSDs vs t) plots give slopes of ∼0.6−0.8. Einstein's equation can thus only be used as an estimation for the upper bound of our oligomer diffusion coefficients, which is $\sim 6 \times 10^{-6}$ cm^2 s^{-1} at a temperature of 400 K. Figure 9a provides a direct comparison of the dynamics of PEO in the absence and presence of the nanoparticle. Like most other simulation results,[35,36,42,43,45,49,51,53] the MSDs are clearly affected by the filler and the dynamics generally slowed. Experimentally, the relaxation dynamics of PEO were found to be slower as well in the presence of silica nanoparticles.[29] Figure 9a also shows the different MSDs as a function of their chemical nature. At short times, backbone MSDs are slower than the end groups. Indeed, the most mobile groups are the $-CH_3$, followed by the more polar −OH.

To see the actual effect of the interface on the dynamics, the MSDs have been calculated as a function of R. The results can be found in Figure 9b for a time interval of 100 ps. For all species concerned, the mobility is obviously strongly reduced at the interface. This is consistent with the reduction in mobility of adsorbed polymer segments along the nanoparticle surface shown by Smith et al.,[45] as well as the gradual slower relaxation time of the scattering function for the layers closest to the filler reported by Starr et al.[42,43] in the case of attractive nanoparticle−polymer interactions. Similar observations have been made with the generic model of Brown et al.,[49] while their fully atomistic model of PBMA showed a reduction close to the interface but a slight enhancement in the interphase region due to the particular density profile found.[50] The dynamic effect of the more flexible PEO oligomers displayed in Figure 9b spans a larger distance than the actual structural changes and gets progressively less pronounced when R increases. Eventually, it returns to the pure melts values around 40 Å, as shown by the straight lines of Figure 9b. Very similar findings have been reported by Borodin et al. for PEO at a planar crystalline TiO_2 interface.[53]

It is worth noting that the methyl end groups always seem to be more mobile than the hydroxyl end groups which, despite the dynamic exchanges in the hydrogen-bonding sphere noted above, have a tendency to remain in the immediate vicinity of the filler. The rare backbone O moieties, which come within this sphere of influence, are also immobilized by the silica nanoparticle through hydrogen bonds. Indeed, at low R, the backbone O and the −OH MSDs become of the same order of magnitude than the silanol hydrogens.

3.8. Conformational Dynamics. To try and evaluate the possible effects of the presence of the nanoparticle on the trans−gauche interconversion dynamics of backbone torsional modes, relaxation functions of the form

$$R_{AB}(t) = \langle H_A\{\tau_i(0)\} H_B\{\tau_i(t)\} \rangle \qquad A = G^-, T, G^+ \text{ and } B = G^-, T, G^+ \quad (8)$$

were computed. In eq 8, $\tau_i(t)$ is the value of dihedral angle i at time t and $H_A\{\tau_i(t)\}$ is the characteristic function of the A (=G^-, T, or G^+) state. Each characteristic function takes only two values:

$$H_T\{\tau_i(t)\} = 1, \quad \text{if } -60° \le \tau_i(t) \le 60°; \quad \text{otherwise, } H_T\{\tau_i(t)\} = 0 \quad (9)$$

$$H_{G^-}\{\tau_i(t)\} = 1, \quad \text{if } -180° \le \tau_i(t) < -60°; \quad \text{otherwise, } H_{G^-}\{\tau_i(t)\} = 0 \quad (10)$$

$$H_{G^+}\{\tau_i(t)\} = 1, \quad \text{if } 60° < \tau_i(t) \le 180°; \quad \text{otherwise, } H_{G^+}\{\tau_i(t)\} = 0 \quad (11)$$

The technique has been presented in detail elsewhere[89] and provides a reliable method for assessing the degree of conformational equilibrium in a system and the rate at which it is attained. Note that the initial values of the relaxation functions are $R_{AB}(0) = 0$ if A ≠ B and $R_{AB}(0) = \langle X_A \rangle$, i.e. the mean fraction of conformers in state A, if A = B. If a conformational equilibrium can be established within the simulation time scale, then $R_{AB}(t)$ tends to the product $\langle X_A \rangle \langle X_B \rangle$. All nine possible permutations of the $R_{AB}(t)$ relaxation functions were computed from the last 1 ns of each production run for the C−C−O−C and O−C−C−O backbone torsions using the configurations stored at 5 ps intervals. For the C−C−O−C torsions, the relaxation functions decayed smoothly to their expected limiting values within ∼200 ps. The relaxation functions for the O−C−C−O torsions also decayed smoothly but on a time scale ∼3 times slower, as has been seen before,[56] due the higher energy barriers.[90] Rather than present all these functions, we concentrate on just one for each significant torsion, $R_{TT}(t)$ for C−C−O−C torsions and $R_{GG}(t)=(R_{G^-G^-}(t) + R_{G^+G^+}(t))/2$ for O−C−C−O torsions. This choice corresponds to the initial state being the most populated in each case. These $R_{AA}(t)$ relaxation functions were then normalized to give their corresponding correlation functions, $C_{AA}(t)$, using the following expression:

$$C_{AA}(t) = \frac{R_{AA}(t) - \langle X_A \rangle^2}{\langle X_A \rangle - \langle X_A \rangle^2} \quad (12)$$

The resulting $C_{AA}(t)$ values were found to fit well to the stretched exponential (Kohlrausch−Williams−Watts) functional form:

$$C_{AA}(t) = \exp\left(-\left(\frac{t}{\alpha}\right)^{\beta}\right) \quad (13)$$

Best fit values for α and β were obtained using nonlinear least squares regression over the range from $t = 0$ up to where the functions decayed to values of ∼0.1. The corresponding relaxation times were then obtained from the analytic time integral of the stretched exponential:

$$\tau_{AA} = \int_0^\infty \exp\left(-\left(\frac{t}{\alpha}\right)^{\beta}\right) dt = \frac{\alpha}{\beta}\int_0^\infty s^{1/\beta - 1} \exp(-s)\, ds = \frac{\alpha}{\beta}\Gamma\left(\frac{1}{\beta}\right) \quad (14)$$

where the Γ function was estimated to high precision using a standard numerical technique.[91]

The overall values of τ_{TT} and τ_{GG} for the C−C−O−C and O−C−C−O torsions, respectively, are given for each system simulated in Table 3. Errors in τ_{TT} tend to be higher than those for τ_{GG} as the configuration storing interval of 5 ps leads to effectively fewer data points in the region where most of the decay occurs in the correlation functions. In general, however, the relaxation times increase significantly when $-CH_3$ end groups are replaced by −OH or when the silica nanoparticle is added. Predictions for the relaxation times of the equimolar mixture systems have been made from the average relaxation functions of the two pure systems and these are also given, in italics, in Table 3. The reliability in the case of C−O−C−C torsions is somewhat compromised by the larger errors but in the case of O−C−C−O the ideal prediction of τ_{GG} for the pure equimolar fluid is in very good agreement with the actual value found in the **peo3** system. When the silica is added to this latter system, the ideal prediction slightly underestimates the actual τ_{GG} but a visual inspection of the curves (not shown) reveals that they practically coincide with no systematic differences.

To try to understand the general increase in relaxation times, the relaxation functions have also been calculated as a function of R. Previous work has shown that these functions are sensitive to the proximity of the interface.[49] Similar findings have also been reported for the autocorrelation function for the cosine of the torsion angle (TACF) by Borodin et al. for PEO at a planar TiO_2 interface.[53] To calculate the relaxation functions, torsion angles were assigned, at each point in time, to radial shells of 5 Å thickness starting from $R = 14$ Å, i.e. in correspondence with the peaks seen in the radial mass density (Figure 3). This assignment was based on the center-of-mass of the four atoms involved in the torsion. As there is no guarantee with time that the angles stay in the same zone, a dihedral angle was included in the statistics of a given layer as long as it remained there, at least as best as could be determined within the 5 ps resolution of the stored configurations. At long time intervals, this presents a problem of statistics as there become fewer and fewer angles which have not wandered out of their initial layer at some point. However, in agreement with the diffusion results, angles closer to the nanoparticle remained noticeably longer in the same layer than those further away. For example, for all the silica-containing systems, about half of the angles in the first layer ($14 \le R < 19$ Å) at a particular time origin stay there for 500 ps, whereas for the second layer ($19 \le R < 24$ Å), only one-tenth of them remain. For greater R, practically all angles left their initial layer at least once in 500 ps. Another problem with this selective averaging of time correlation functions has been pointed out by Borodin et al.[53] A bias can be introduced into the results by the manner in which only those (slowly diffusing) angles staying in the same layer are contained in the averages. They found that for the C−C−O−C angles in the pure fluid of PEO chains, the selective averaging in slabs of width 4.2 Å gave TACFs that decayed marginally slower than the normal indiscriminate averaging.[53] Tests were made here on our shorter oligomer pure melts, using the center-of-mass of the system as an arbitrary reference point for the radial vector and the same 5 Å zone widths as for the nanoparticle containing simulations. They revealed that the average C−C−O−C $R_{TT}(t)$ relaxation functions, duly weighted according to average occupancy, from the zones between 14 and 49 Å were also biased in a similar way toward slower relaxation.

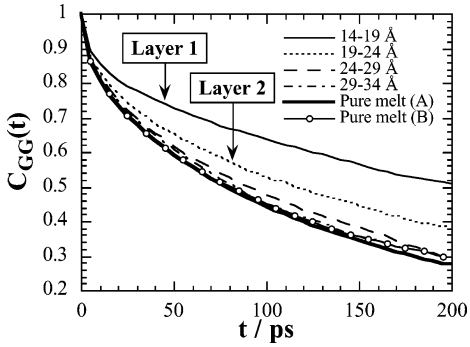

Figure 10. Normalized relaxation functions for the gauche states of OCCO torsions at different distances from the center-of-mass of the nanoparticle for the **peosil1** system. Four zones are shown from 14 to 34 Å at 5 Å intervals as well as the same function obtained from the corresponding pure melt system (**peo1**) in two different ways: (A) using the usual indiscriminate averaging of all angles and (B) averaging as for the nanoparticle only over angles which remain in the same spherical layers of thickness 5 Å.

However, the much slower relaxing $R_{GG}(t)$ functions for the O−C−C−O torsions were, within error, the same as those obtained when averaging indiscriminately over all angles. This suggests greater coupling between translational and conformational modes in the case of the faster relaxing C−C−O−C torsions.

An example of the results obtained for the relaxation functions is shown in Figure 10 where the normalized function $C_{GG}(t)$ for O−C−C−O torsions is presented for four different regions around the center-of-mass of the nanoparticle in the **peosil1** system. For comparison, the same function obtained for the pure dimethyl PEO melt (**peo1**) by indiscriminate averaging is also shown in Figure 10 as well as the $C_{GG}(t)$ obtained when using the same selective averaging in spherical layers as for the nanocomposite system. The good agreement between the latter two confirms the unimportance of the biased averaging in the case of O−C−C−O torsions, at least for the given conditions of temperature and pressure.

Results (not shown) for the O−C−C−O torsions in the other two silica-containing systems and for the $C_{TT}(t)$ function of C−C−O−C torsions demonstrate clearly, and despite the known bias in the latter case, that conformational relaxation is significantly slowed in the first layer. In the example shown in Figure 10, the τ_{GG} relaxation time of the first layer, obtained in the same manner as explained above, is tentatively estimated to be ∼1000 ps; the limited decay in the function leads to considerable uncertainty in the resulting relaxation time. This value is at least four times longer than the value of 231 ± 2 ps for the pure melt and it is certainly a more dramatic effect than was seen in the case of a generic polymer next to a completely repulsive nanoparticle.[49] Slowing down of a similar order though has been found previously for the TACFs of PEO in the first layer next to a TiO_2 surface.[53]

In this work, the second layer is also clearly affected in Figure 10 but certainly to a lesser extent than the first, τ_{GG} = 250 ± 5 ps. Considering all the results obtained for the region between 24 and 34 Å, i.e., ∼10−20 Å from the interface, it can be said that there is a systematic tendency for a slight slowing down also. Beyond that distance though, the conformational relaxation is indistinguishable from the limiting results for the pure melt. The range of the effect of the nanoparticle on conformational relaxation thus confirms that found for translational diffusion, i.e., it extends to at least 20 Å from the interface.

4. Conclusion

Fully atomistic equilibrium MD simulations of bulk melt pure PEO oligomers and PEO oligomer−silica systems have been performed with two types of chain differing simply in their end groups. Despite their fully atomistic description and the rough surface of the silica nanoparticle, many characteristics of our models were in agreement with those of simulations carried out with coarser-grained models.[35,36,40,43,45,46,49] However, they differed from other atomistically detailed MD simulations carried out on PBMA−silica systems,[50,51] in that our PEO oligomers were in the melt. They were thus fully able to come to equilibrium, which facilitated the comparison of end group effects. Many similarities were found with a different longer-chain model of PEO in contact with a planar crystalline TiO_2 surface.[53]

Most properties under study in the PEO−silica systems were found to be significantly affected close to the silica surface with a relatively rapid return to bulk melt values over a range of influence spanning approximately 10−15 Å for static and 20−30 Å for dynamic properties. Overall average structural properties were thus only slightly changed as the volume fraction of the perturbed PEO was relatively small. However, those PEO molecules in the immediate vicinity of the silica nanoparticle were clearly arranged in densely packed shells, stabilized by the added PEO−silica attractions. Conformations in the first layer changed in order to better adapt to the filler structure and the backbones also adopted flattened parallel alignments with respect to the silica surface. The methyl end groups did not show special characteristics other than their steric effect. On the other hand, hydroxyl end groups tended to position themselves perpendicular to the surface, in agreement with experimental evidence.[14,19,20,27] thus leading to very efficient hydrogen-bonding between the hydroxyl oxygens and the silanol hydrogens. This much higher affinity of the −OH end groups with respect to the methyl counterparts was reflected in a low diffusion close to the interface and was clearly demonstrated in the equimolar mixture. Translational diffusion in general was reduced close to the interface and the rate of conformational relaxation was significantly slowed.

Even though only one chain length has been studied here, previous results for chain melts at planar interfaces[88] and scaling arguments[92] suggest strongly that the range of influence of the nanoparticle will not change significantly if longer chains were used. In this respect, we believe that the association made in similar polymer melt studies between the range of influence and the mean square radius of gyration of the chains is slightly misleading.[42,43] albeit more justifiable in the case of polymer solutions.[10,92] In any case, actually establishing the chain length dependence of the range of influence is difficult to verify using simulation as relaxation times increase rapidly with chain length rendering the attainment of equilibrium for significantly longer chains, e.g., a factor of 10, rather costly in terms of CPU time.

This study is well representative of the current possibilities and difficulties encountered when applying fully atomistic molecular dynamics simulations to oligomer−nanoparticle systems. Although the preparation procedure is complex and time-consuming, a lot of

information can be obtained in order to complement experimental evidence. For example, in the specific case of PEO−silica systems, it would be interesting at a later stage to add a third phase to our models, i.e., water which is known to compete with PEO for the silanols.[4,28] Its effect on both PEO and the PEO−silica interface could be tackled using a similar approach to that presented here.

Acknowledgment. The CINES (Montpellier, France) and the IDRIS (Orsay, France) supercomputing centers are acknowledged for provision of computer time, as well as the University of Savoie (Le Bourget-du-Lac, France) and the Rhône-Alpes region for the provision of COMPAQ DS20E servers.

References and Notes

(1) Napper, D. H. *Polymeric Stabilization of Colloidal Dispersions*; Academic Press: New York, 1983.
(2) Fleer, G. J.; Stuart, M. A. C.; Scheutjens, J. M. H. M.; Cosgrove, T.; Vincent, B. *Polymers at Interfaces*; Chapman and Hall: London, 1993.
(3) Van der Beek, G. P.; Cohen Stuart, M. A.; Cosgrove, T. *Langmuir* **1991**, *7*, 327.
(4) Hasan, F. B.; Huang, D. D. *J. Colloid Interface Sci.* **1997**, *190*, 161.
(5) Mathur, S.; Brij, M.-M. *J. Colloid Interface Sci.* **1997**, *196*, 92.
(6) Lafuma, F.; Wong, K.; Cabane, B. *J. Colloid Interface Sci.* **1991**, *143*, 9.
(7) Liu, S. F.; Legrand, V.; Gourmand, M.; Lafuma, F.; Audebert, R. *Colloids Surf. A: Physicochem. Eng. Aspects* **1996**, *111*, 139.
(8) Chaplain, V.; Janex, M. L.; Lafuma, F.; Graillat, C.; Audebert, R. *Colloid Polym. Sci.* **1995**, *273*, 984.
(9) Van der Beek, G. P.; Cohen Stuart, M. A.; Fleer, G. J.; Hofman, J. E. *Macromolecules* **1991**, *24*, 6600.
(10) Cosgrove, T.; Griffiths, P. C.; Lloyd, P. M. *Langmuir* **1995**, *11*, 1457.
(11) Neel, O.; Ducouret, G.; Lafuma, F. *J. Colloid Interface Sci.* **2000**, *230*, 244.
(12) Killmann, E.; Sapuntzjis, P.; Fleer, G. C.; Tadros, T. F. E.; Cosgrove, T. *Colloids Surf. A: Physicochem. Eng. Aspects* **1994**, *86*, 229.
(13) Boissier, C.; Löfroth, J. E.; Nyden, M. *Langmuir* **2002**, *18*, 7313.
(14) Trens, P.; Denoyel, R. *Langmuir* **1993**, *9*, 519.
(15) Dijt, J. C.; Stuart, M. A. C.; Fleer, G. J. *Macromolecules* **1994**, *27*, 3219.
(16) Griffiths, P. C.; Stilbs, P. *Langmuir* **1995**, *11*, 898.
(17) Fu, Z.; Santore, M. M. *Macromolecules* **1998**, *31*, 7014.
(18) Wind, B.; Killmann, E. *Colloid Polym. Sci.* **1998**, *276*, 903.
(19) Bjelopavlic, M.; Singh, P. K.; El-Shall, H.; Moudgil, B. M. *J. Colloid Interface Sci.* **2000**, *226*, 159.
(20) Zaman, A. A.; Bjelopavlic, M.; Moudgil, B. M. *J. Colloid Interface Sci.* **2000**, *226*, 290.
(21) Mubarekyan, E.; Santore, M.-M. *Macromolecules* **2001**, *34*, 4978.
(22) Fu, Z.; Santore, M. M. *Langmuir* **1998**, *14*, 4300.
(23) Huang, Y.; Santore, M. M. *Langmuir* **2002**, *18*, 2158.
(24) Fu, Z.; Santore, M. M. *Langmuir* **1997**, *13*, 5779.
(25) Esumi, K.; Iitaka, M.; Koide, Y. *J. Colloid Interface Sci.* **1998**, *208*, 178.
(26) Campbell, A.; Somasundaran, P. *J. Colloid Interface Sci.* **2000**, *229*, 257.
(27) Zaman, A. A. *Colloid Polym. Sci.* **2000**, *278*, 1187.
(28) Chen, C.-Y.; Even, M. A.; Wang, J.; Chen, Z. *Macromolecules* **2002**, *35*, 9130.
(29) Zhang, Q.; Archer, L. A. *Langmuir* **2002**, *18*, 10435.
(30) Allen, M. P.; Tildesley, D. J. *Computer Simulation of Liquids*; Clarendon Press: Oxford, England, 1987.
(31) Frenkel, D.; Klein, M.; Parrinello, M.; Smit, B. *Understanding Molecular Simulation*, 2nd ed.; Academic Press: San Diego, CA, and London, 2002.
(32) Frankland, S. J. V.; Harik, V. M.; Odegard, G. M.; Brenner, D. W.; Gates, T. S. *Compos. Sci. Technol.* **2003**, *63*, 1655.
(33) Huh, J.; Ginzburg, V.-V.; Balazs, A.-C. *Macromolecules* **2000**, *33*, 8085.
(34) Wang, Q.; Nealey, P. F.; De Pablo, J. J. *J. Chem. Phys.* **2003**, *118*, 11278.
(35) Vacatello, M. *Macromolecules* **2001**, *34*, 1946.
(36) Vacatello, M. *Macromol. Theory Simul.* **2002**, *11*, 501.
(37) Vacatello, M. *Macromolecules* **2002**, *35*, 8191.
(38) Vacatello, M. *Macromol. Theory Simul.* **2002**, *11*, 53.
(39) Vacatello, M. *Macromolecules* **2003**, *36*, 3411.
(40) Vacatello, M. *Macromol. Theory Simul.* **2003**, *12*, 86.
(41) Feng, J.; Ruckenstein, E. *Polym. Guildford* **2003**, *44*, 3141.
(42) Starr, F. W.; Schrøder, T. B.; Glotzer, S. C. *Phys. Rev. E* **2001**, *64*, 021802.
(43) Starr, F. W.; Schrøder, T. B.; Glotzer, S. C. *Macromolecules* **2002**, *35*, 4481.
(44) Starr, F.-W.; Douglas, J.-F.; Glotzer, S.-C. *J. Chem. Phys.* **2003**, *119*, 1777.
(45) Smith, G.-D.; Bedrov, D.; Li, L.; Byutner, O. *J. Chem. Phys.* **2002**, *117*, 9478.
(46) Smith, J. S.; Bedrov, D.; Smith, G. D. *Compos. Sci. Technol.* **2003**, *63*, 1599.
(47) Kasemägi, H.; Klintenberg, M.; Aabloo, A.; Thomas, J.-O. *J. Mater. Chem.* **2001**, *11*, 3191.
(48) Kasemägi, H.; Klintenberg, M.; Aabloo, A.; Thomas, J.-O.; De Leeuw, S. W. *Solid State Ionics* **2002**, *147*, 367.
(49) Brown, D.; Mélé, P.; Marceau, S.; Albérola, N. *Macromolecules* **2003**, *36*, 1395.
(50) Brown, D.; Marceau, S.; Mélé, P.; Albérola, N. D. In *Proceedings of Eurofillers 2003, Alicante, Spain, Sep 8−11* 2003; Martín Martínez, J. M., Ed.; University of Alicante: Alicante, Spain.
(51) Marceau, S. Ph.D. Thesis, University of Savoie, 2003.
(52) Frith, W. J.; Strivens, T. A.; Mewis, J. *J. Colloid Interface Sci.* **1990**, *139*, 55.
(53) Borodin, O.; Smith, G. D.; Bandyopadhyaya, R.; Byutner, O. *Macromolecules* **2003**, *36*, 7873.
(54) Brown, D. *The gmq User Manual Version 3*; 1999; available at http://www.univ-savoie.fr/labos/lmpc/db.html.
(55) Neyertz, S.; Brown, D.; Thomas, J. O. *J. Chem. Phys.* **1994**, *101*, 10064.
(56) Neyertz, S.; Brown, D. *J. Chem. Phys.* **1995**, *102*, 9725.
(57) Neyertz, S.; Brown, D.; Colombini, D.; Albérola, N. D.; Merle, G. *Macromolecules* **2000**, *33*, 1361.
(58) Smith, G. D.; Yoon, D. Y.; Jaffe, R. L.; Colby, R. H.; Krishnamoorti, R.; Fetters, L. J. *Macromolecules* **1996**, *29*, 3462.
(59) Ryckaert, J.-P. *Mol. Phys.* **1985**, *55*, 549.
(60) Hammonds, K. D.; Ryckaert, J.-P. *Comput. Phys. Comm.* **1991**, *62*, 336.
(61) Matsuura, H.; Fukuhara, K. *J. Polym. Sci., Part B: Polym. Phys.* **1986**, *24*, 1383.
(62) Rappé, A. K.; Casewit, C. J.; Colwell, K. S.; Goddard, W. A., III.; Skiff, W. M. *J. Am. Chem. Soc.* **1992**, *114*, 10024.
(63) Brown, D.; Neyertz, S. *Mol. Phys.* **1995**, *84*, 577.
(64) Takahashi, Y.; Tadokoro, H. *Macromolecules* **1973**, *6*, 672.
(65) Ewald, P. P. *Ann. Phys.* **1921**, *64*, 253.
(66) Smith, W. *Comput. Phys. Comm.* **1992**, *67*, 392.
(67) Jorgensen, W. L. *J. Phys. Chem.* **1986**, *90*, 1276.
(68) Stubbs, J. M.; Chen, B.; Potoff, J. J.; Siepmann, J. I. *Fluid Phase Equilib.* **2001**, *183−184*, 301.
(69) Frisch, M. J.; Trucks, G. W.; Schlegel, H. B.; Scuseria, G. E.; Robb, M. A.; Cheeseman, J. R.; Zakrzewski, V. G.; Montgomery, J. A., Jr.; Stratmann, R. E.; Burant, J. C.; Dapprich, S.; Millam, J. M.; Daniels, A. D.; Kudin, K. N.; Strain, M. C.; Farkas, O.; Tomasi, J.; Barone, V.; Cossi, M.; Cammi, R.; Mennucci, B.; Pomelli, C.; C. Adamo; Clifford, S.; Ochterski, J.; Petersson, G. A.; Ayala, P. Y.; Cui, Q.; Morokuma, K.; Malick, D. K.; Rabuck, A. D.; Raghavachari, K.; Foresman, J. B.; Cioslowski, J.; Ortiz, J. V.; Baboul, A. G.; Stefanov, B. B.; Liu, G.; Liashenko, A.; Piskorz, P.; Komaromi, I.; Gomperts, R.; Martin, R. L.; Fox, D. J.; Keith, T.; Al-Laham, M. A.; Peng, C. Y.; Nanayakkara, A.; Gonzalez, C.; Challacombe, M.; Gill, P. M. W.; Johnson, B.; Chen, W.; Wong, M. W.; Andres, J. L.; Gonzalez, C.; Head-Gordon, M.; Replogle, E. S.; Pople, J. A. *Gaussian 98*; Gaussian Inc.; Pittsburgh, PA, 1998.
(70) Singh, U. C.; Kollman, P. A. *J. Comput. Chem.* **1984**, *5*, 129.
(71) Neyertz, S.; Brown, D. *J. Chem. Phys.* **1996**, *104*, 10063.
(72) Neyertz, S.; Brown, D. *J. Chem. Phys.* **2001**, *115*, 708.
(73) Roe, R. J. *J. Phys. Chem.* **1968**, *72*, 2013.
(74) Van Krevelen, D. W. *Properties of polymers: their correlation with chemical structure; their numerical estimation and prediction from additive group contributions*, 3rd completely revised ed.; Elsevier: Amsterdam, 1990.

(75) Brown, D.; Clarke, J. H. R. *Comput. Phys. Comm.* **1991**, *62*, 360.
(76) Fincham, D. *Mol. Simul.* **1994**, *13*, 1.
(77) Berendsen, H. J. C.; Postma, J. P. M.; van Gunsteren, W. F.; DiNola, A.; Haak, J. R. *J. Chem. Phys.* **1984**, *81*, 3684.
(78) Van Beest, B. W. H.; Kramer, G. J.; van Santen, R. A. *Phys. Rev. Lett.* **1990**, *64*, 1955.
(79) Brodka, A.; Zerda, T. W. *J. Chem. Phys.* **1996**, *104*, 6319.
(80) Berendsen, H. J. C.; Grigera, J. R.; Straatsma, T. P. *J. Phys. Chem.* **1987**, *91*, 6269.
(81) Heyes, D. M. *J. Chem. Soc., Faraday Trans.* **1994**, *90*, 3039.
(82) Zhuravlev, L. T. *Colloids Surf. A: Physicochem. Eng. Aspects* **2000**, *173*, 1.
(83) Wypych, G. *Handbook of Fillers*, 2nd ed.; ChemTec Publishing & William Andrew Inc.: Toronto, Ontario, Canada, and Norwich, NY, 1999.
(84) Eliassi, A.; Modarress, H.; Mansoori, G. A. *J. Chem. Eng. Data* **1998**, *43*, 719.
(85) *Polymer Handbook*, 3rd ed.; Wiley-Interscience: New York, 1989.
(86) Müller-Plathe, F.; van Gunsteren, W. F. *Macromolecules* **1994**, *27*, 6040.
(87) Müller-Plathe, F. *Acta Polym.* **1994**, *45*, 259.
(88) Bitsanis, I.; Hadziioannou, G. *J. Chem. Phys.* **1990**, *92*, 3827.
(89) Brown, D.; Clarke, J. H. R. *J. Chem. Phys.* **1990**, *92*, 3062.
(90) Gejji, S. P.; Tegenfeldt, J.; Lindgren, J. *Chem. Phys. Lett.* **1994**, *226*, 427.
(91) Lanczos, C. *SIAM J. Numer. Anal.* **1964**, *B1*, 86.
(92) De Gennes, P.-G. *Scaling Concepts in Polymer Physics*; Cornell University Press: Ithaca, NY, 1979.

MA0359537